



1 **Altered Seasonal Sensitivity of Net Ecosystem Exchange to Controls** 2 **Driven by Nutrient Balances in a Semi-arid Savanna**

3
4 Laura Nadolski^{1,2}, Tarek S. El-Madany¹, Jacob Nelson¹, Arnaud Carrara³, Gerardo Moreno⁴, Richard Nair⁵, Yunpeng Luo⁶, Anke
5 Hildebrandt^{2,7}, Victor Rolo⁴, Markus Reichstein¹, Sung-Ching Lee¹

6 ¹Biogeochemical Integration, Max-Planck Institute for Biogeochemistry, Jena, Germany

7 ²Faculty of Chemistry and Earth Science, Friedrich-Schiller University, Jena, Germany

8 ³Fundacion Centro de Estudios Ambientales del Mediterráneo (CEAM), Valencia, Spain

9 ⁴Faculty of Forestry, Institute of Dehesa Research (INDEHESA), Universidad de Extremadura, Plasencia 10600, Spain

10 ⁵Discipline of Botany, School of Natural Sciences, Trinity College Dublin, Dublin Ireland

11 ⁶Swiss Federal Institute for Forest, Snow and Landscape Research WSL, 8903 Birmensdorf, Switzerland

12 ⁷Department Computational Hydrosystems, Helmholtz Centre for Environmental Research (UFZ), Leipzig, Germany

13 *Correspondence to:* Laura Nadolski (lnadolski@bgc-jena.mpg.de)

14 **Abstract**

15 Semi-arid ecosystems dominate variability and trend of the terrestrial carbon sink. They are sensitive to environmental changes
16 following anthropogenic influence, such as an altered ratio of nitrogen (N) to phosphorus (P) due to increasing N deposition.
17 Semi-arid savannas with different vegetation compositions have complex carbon dynamics, and their responses to
18 environmental change are not yet well understood. We analysed a long-term (2016-2022/2023) dataset of flux,
19 biometeorological and vegetation data (satellite and ground measurements) of a manipulated semi-arid savanna to reveal how
20 altered nutrient levels and stoichiometric balance affect the seasonal sensitivity of net ecosystem exchange (NEE) to its drivers.
21 We used the Singular Spectrum Analysis to extract the seasonal signal of all variables and assessed the key drivers of NEE
22 over the study period as a whole and in different seasons, using Pearson correlation and Information Theory. We found that
23 both N and N+P addition to the ecosystem increased seasonal NEE variability, driven by greenness of the herbaceous layer.
24 Analysing 7 years of data together, the water limitation in summer and energy limitation in winter outcompeted the fertilization
25 effect. By investigating different phenological seasons, effects of nutrient addition on NEE-control relationships became
26 clearer. In the summer, N+P addition led to a potential change in species composition and productivity resulting in a stronger
27 interaction between herbaceous layer and NEE. During the transitional seasons (i.e., drydown and regreening), which
28 determine the senescence and regreening of the herbaceous layer, we found NEE to be less sensitive towards meteorological
29 drivers like relative humidity, radiation and air temperatures with N addition. The increasing NEE variability might become
30 even more pronounced with N deposition and a changing climate in the future.



31 **1 Introduction**

32 Terrestrial ecosystems are a major component of the global carbon cycle, with the ability to store significant amounts of carbon
33 (Friedlingstein et al., 2022). While forests and wetlands contribute most to the terrestrial carbon sink, semi-arid ecosystems
34 dominate its trend and interannual variability (Ahlström et al., 2015; Poulter et al., 2014; Zhang et al., 2016). Semi-arid
35 ecosystems typically take up carbon from the atmosphere during the wet season and are dormant or emit carbon during the dry
36 season (Metz et al., 2023). Net ecosystem exchange (NEE) describes this balance between carbon uptake through
37 photosynthesis, typically expressed as gross primary productivity (GPP), and carbon release through ecosystem respiration
38 (R_{eco}). NEE in semi-arid regions varies strongly from year to year, depending on the climatic conditions and water availability
39 (Haverd et al., 2017; Piao et al., 2020).

40 Despite their important role in the global carbon cycle, semi-arid ecosystems and their dynamics are still not well understood.
41 Long-term in-situ measurements from these regions are scarce. Particularly, eddy covariance (EC) measurements, which
42 provide high-frequency and continuous ecosystem trace gas and water flux data (Baldocchi, 2020), are underrepresented in
43 these regions (Jung et al., 2020). Consequently, semi-arid ecosystems remain poorly represented in terrestrial biosphere models
44 (Fawcett et al., 2022; MacBean et al., 2021) due to their complex structure and high spatio-temporal variability, which are
45 difficult to generalize.

46 Recently efforts have been made to reveal drivers of NEE in semi-arid savannas to understand better their role in the global
47 carbon cycle (Baldocchi and Arias Ortiz, 2024; Kannenberg et al., 2024; Ma et al., 2007, 2016; Zhang et al., 2010). Water
48 related variables like precipitation and soil moisture availability are amongst the main NEE drivers (Archibald et al., 2009;
49 Baldocchi and Arias Ortiz, 2024; Del Grosso et al., 2018; Huang et al., 2016b; Morgan et al., 2016), as they promote plant
50 photosynthesis (Parton et al., 2012) and enhance heterotrophic respiration rates (Ma et al., 2016). Furthermore,
51 photosynthetically active radiation (PAR), vapor pressure deficit (VPD) and air temperatures can strongly impact NEE
52 (Archibald et al., 2009; Baldocchi and Arias Ortiz, 2024; Del Grosso et al., 2018). Light absorption propels the electron
53 transport mechanism integral to photosynthesis. VPD influences the modulation of stomata opening and temperature impacts
54 the kinetics of enzymes involved in carboxylation processes, the process of carbon uptake into the plant (Baldocchi and Arias
55 Ortiz, 2024). Also, other biotic factors, like soil microbial communities and organic matter play an important role in the
56 ecosystem carbon cycle and contribute to R_{eco} (Austin and Vivanco, 2006; Bastida et al., 2016; Hu et al., 2014). These drivers
57 can differ for different vegetation types. Typical ecosystems in semi-arid regions are savannas where coexisting vegetation
58 layers (e.g., tree and grass) interact in complex ways. The layers differ in their rooting depths (Moreno et al., 2005; Rolo and
59 Moreno, 2012), water use strategies (Cubera and Moreno, 2007; Miller et al., 2010; Steiner et al., 2024) and phenological and
60 life cycle strategies (Whitecross et al., 2017). Especially the herbaceous vegetation in two-layer ecosystems is often
61 underestimated in its importance for the ecosystem water and carbon fluxes (Dubbart et al., 2014). In the Iberian Peninsula
62 *dehesas* (or *montados* in Portugal), human shaped savanna-like agroecosystem, are wide-spread (Den Herder et al., 2017).
63 *Dehesas* are open oak woodlands with an herbaceous layer that consists mainly of annual grasses and sometimes crops. The



64 tree layer is evergreen (Moreno, 2008), whereas the herbaceous layer typically follows an annual cycle of growth, senescence
65 and regreening (Ma et al., 2007; Perez-Priego et al., 2015). As savannas are typically characterized by changing resource
66 limitations throughout the year (Luo et al., 2020; Ries and Shugart, 2008), limited by water in the dry season and by nutrients
67 and energy in the wet season (Moreno, 2008; Morris et al., 2019; Nair et al., 2019), these drivers change with the seasons
68 throughout the year. The complex interactions between tree and grass layers, along with changing limitations result in a high
69 complexity of the ecosystem's carbon dynamics, which remain to be fully understood.

70 Semi-arid ecosystems face numerous human-induced environmental changes, including stoichiometric imbalances between
71 nitrogen (N) and phosphorus (P). These imbalances arise from increasing N inputs into ecosystems due to fertilizers and
72 combustion of fossil fuels (Steffen et al., 2015) without corresponding increase in P inputs (Penuelas et al., 2013). Few studies
73 have dealt so far with the impact of altered nutrient levels on NEE and its drivers in semi-arid regions. The availability and
74 stoichiometric balance of N and P influences ecosystem functioning and plant traits (Reichstein et al., 2014), water use
75 efficiency (El-Madany et al., 2021; Huang et al., 2016a), canopy structure (Migliavacca et al., 2017), composition of species
76 (Sardans et al., 2012), and the seasonality of vegetation activity (Luo et al., 2020). However, different plant types react
77 differently to changes in nutrient availability, due to variations in generation times and buffering capacities (Pardo et al., 2011).
78 Therefore, the understanding of the response of complex tree-grass ecosystems to changes in N and P availability and their
79 stoichiometric balance is still poor.

80

81 In this study we took advantage of the unique long-term dataset collected in a semi-arid *dehesa*, Majadas de Tiétar, in South-
82 Western Spain. A large-scale nutrient addition experiment has been running here since 2015, providing an exceptional
83 opportunity to study the long-term influence of altered N:P ratios on ecosystem functioning (El-Madany et al., 2021). Three
84 EC flux towers have been set up, with the footprint of one tower receiving N fertilization, another one receiving N+P
85 fertilization and the third serving as control. Previous studies found that both treatments increased the annual carbon uptake of
86 the ecosystem and that N+P addition increased the water use efficiency of the ecosystem more than N-only addition, which
87 could be attributed to higher transpiration rates and a changed root strategy in the N-only fertilized plot (El-Madany et al.,
88 2021; Nair et al., 2019). Nutrient addition further led to a higher seasonal amplitude of maximum GPP and a faster increase
89 during the regreening period, but also a faster senescence during the drydown period, which indicates changes in plant structure
90 and physiology (Luo et al., 2020).

91 Here we analysed a 7-year (2016-2022) timeseries of daily values of environmental and biogenic variables from Majadas de
92 Tiétar, combining flux data, meteorological measurements, digital repeat photography and satellite data to address the
93 following questions: How do altered nutrient levels and stoichiometric balance affect

- 94 – annual NEE and its variability in a semi-arid savanna?
- 95 – the relationship between NEE and its key controls?
- 96 – the relationship between NEE and its key controls in different seasons?
- 97 – the sensitivity of NEE to its controls over time?



98 The relationships between NEE and its controls vary across different time scales (Mahecha et al., 2007). To disentangle these
99 timescales from a time series and eliminate noise from the high-frequency measurements, we can use decomposition methods
100 (Linscheid et al., 2020). On short timescales the NEE sensitivity follows the diurnal cycle of the sun, showing a great
101 dependency on radiation. Ecosystem-level responses, in contrast, often develop on scales of months, seasons or years (Ma et
102 al., 2016). Therefore, we extracted the seasonal signals of all variables from the timeseries with the Singular Spectrum Analysis,
103 a data-driven timeseries decomposition method. On the seasonal scale we assessed the key drivers of NEE with Pearson
104 correlation coefficient and information theory-based methods, accounting for collinear relationships as well as leading and
105 lagging effects. As NEE controls vary in their importance throughout the year due to a high seasonality of the ecosystem, we
106 split the dataset into phenological seasons defined by vegetation responses to different limitations.

107 **2 Material and Methods**

108 **2.1 Site Description**

109 The Majadas de Tiétar research site is located in Western Spain (39°56'25"N 5°46'29"W). The local ecosystem consists of an
110 herbaceous stratum and scattered evergreen oak trees (98% *Quercus ilex*). The tree density is around 20-25 trees per hectare
111 (El-Madany et al., 2018), the fractional canopy cover of trees is 23 % and the canopy height is on average 8.7 m (Bogdanovich
112 et al., 2021). The tree leaf area index (LAI) is around 0.35 m² m⁻², the grass layer has a peak LAI in spring but is quite spatially
113 heterogeneous at between 0.5 and 2.5 m² m⁻² (Migliavacca et al., 2017). The site is managed and continuously used for grazing
114 livestock at a low density of 0.3 cows per hectare (El-Madany et al., 2018). In the driest months (July - September) the farmers
115 move the cattle to nearby mountain grasslands (personal communication).

116 The climate at the site is semi-arid with an annual precipitation of around 650 mm with strong interannual variability. Almost
117 85 % of the annual precipitation falls in the wet season between October and April, whereas the rest of the year is dry with
118 occasional rains (El-Madany et al., 2021). According to Nair et al. (2024) we defined five different seasons. Spring is the main
119 growing season and usually starts around March and ends in late May. Then the drydown period starts and the grasses start to
120 become senescent due to depletion of soil moisture, increasing temperatures, radiation and vapor pressure deficit. The summer
121 (typically between end of June until end of September) is characterized by long-lasting dryness and a dormant/dead herbaceous
122 layer. With the onset of precipitation (usually in October), the autumn starts and the herbaceous layer regreens (Nair et al.,
123 2024). The winter months (December-February) are energy limited. The onset and offset of the different seasons vary from
124 year to year, depending on water availability and winter temperature (Luo et al., 2020). The mean annual temperature is 16.7°C
125 with an average minimum temperature of -4.7°C and maximum temperature of 41.1°C (between 2004-2019) (El-Madany et
126 al., 2021). Dominant wind directions are West-Southwest and East-Northeast (El-Madany et al., 2018).

127 Three EC towers at ecosystem level were operated simultaneously at the site. The ecosystem is heterogeneous with a high
128 variability in plant species in the herbaceous layer (at scale of centimetres) and tree cover (at scale of meters). It becomes
129 homogeneous on the scales of a few hundreds of meters. The daytime flux footprints of the three towers correspond to the



130 scale being homogeneous and they do not overlap with each other under prevailing meteorological conditions (El-Madany et
131 al., 2018). The control tower (Fluxnet ID: ES-LMa) has been operated since 2003, it is hereafter referred to as CT. The North
132 tower (Fluxnet ID: ES-LM1) was set up at a distance of 450 m from CT in north-western direction and the South tower (Fluxnet
133 ID: ES-LM2) was located 630 m in southern direction from CT (El-Madany et al., 2018). Since 2015 a large-scale fertilization
134 experiment has been conducted at the site, where N fertilizer is added in the footprint of the North tower (hereafter referred to
135 as NT) and N and P fertilizer are applied in the footprint of the South tower (referred to as NPT) (El-Madany et al., 2021).
136 After the initial application of 100 kg N ha⁻¹ and 50 kg P ha⁻¹ in March 2015 and November 2014, respectively, additional N
137 and P addition were applied every 1-2 years with lower doses. Next to each flux tower there is a radiometric tower setup,
138 measuring radiation components above tree and grass layer, alternating every 15 minutes providing half-hourly measurements
139 for each layer.

140 **2.2 Eddy Covariance and Biometeorological Data**

141 Each of the three EC towers continuously measures sensible heat (H), latent heat (LE) and CO₂ flux. Each system is equipped
142 with a R3-50 sonic anemometer (Gill Instruments Limited, Lymington, UK) to measure three-dimensional wind components
143 and sonic temperature, and a LI7200 infra-red gas analyzer (Licor Bioscience, Lincoln, Nebraska, USA) to measure CO₂ and
144 H₂O mixing ratios. The measurement heights are the same at 15 m above ground (El-Madany et al., 2021). The flux and
145 meteorological data were collected as described by El-Madany et al. (2018). The raw high-frequency data was processed with
146 EddyPro v.7.0.9 (Fratini and Mauder, 2014). The post-processing was done in R using the REdDyProc package (Wutzler et al.,
147 2018). The storage corrections of the CO₂-flux were made with profile measurements from seven points on the flux towers. A
148 friction velocity (u*) threshold was applied following Papale et al. (2006) and data with u* values below the defined threshold
149 were removed. Missing and bad quality data were gap-filled (Mauder and Foken, 2011; Reichstein et al., 2005) for calculating
150 the annual budgets. Additional atmospheric variables that we used are air temperature (Ta) and relative humidity (Rh)
151 measured at two heights (2 m and 15 m), vapor pressure deficit (VPD), CO₂-flux (NEE), air pressure (air_press) and friction
152 velocity (ustar). Furthermore, we incorporated radiometric components such as longwave downward radiation (LWDR),
153 shortwave downward radiation (SWDR) and photosynthetically active radiation (PAR). Soil measurements comprised soil
154 water content integrated over the top 20 cm of the soil (SWCn), soil temperature in open pasture (T_{soilSun}) and below oak tree
155 canopy (T_{soilShd}), and soil heat flux in open pasture (SHF_Sun) and below oak tree canopy (SHF_ShD).

156 Some small data gaps existed in meteorological variables and were filled with the average of the remaining two towers and
157 interpolation. However, the PAR sensor at CT had a malfunction over a long period and therefore we used the PAR timeseries
158 from NT to substitute, as the incoming radiation should not differ substantially between the towers (El-Madany et al., 2018).
159 In addition, we calculated Evaporative Fraction (EF) as the ratio between LE and available energy ($EF = LE/(LE+H)$) (Gentine
160 et al., 2007; Tong et al., 2022). EF is a normalized measure of the surface energy partitioning and can serve as diagnostic of
161 vegetation water status (Nutini et al., 2014). We calculated it at half-hourly timesteps from only positive LE and H values to
162 not introduce extreme outliers into the analysis. EF is strongly linked to meteorological variables like soil moisture, VPD and



163 net radiation (Gentine et al., 2007; Tong et al., 2022), but also to vegetation cover and LAI (Gentine et al., 2007). A full
164 overview of analysed variables is shown in Table 1.

165 **2.3 Vegetation indices**

166 We used three different vegetation indices to represent vegetation greenness, derived from in-situ data (Green chromatic
167 coordinates and albedo) and satellite data (Normalized difference vegetation index).

168
169 Green chromatic coordinate (GCC) is an effective measure for describing greenness variation in semi-arid ecosystems (Luo et
170 al., 2018, 2020). We used daily mean GCC values extracted from the RGB images collected by digital cameras (Stardot
171 NetCam 5MP) which were installed at the top of each ecosystem EC tower facing north, collecting images every 30 minutes.
172 The cameras were set up according to the protocol of the PhenoCam network (<https://phenocam.sr.unh.edu/webcam/tools/>)
173 and collect red, blue, green (RGB) images (Luo et al., 2018). GCC was computed as the fraction of green digital numbers
174 (G_{DN}) in relation to the sum of red (R_{DN}), blue (B_{DN}) and green digital numbers (Richardson et al., 2009):

$$175 \quad GCC = \frac{G_{DN}}{R_{DN} + B_{DN} + G_{DN}} \quad (1)$$

176
177 At each site we selected two regions of interest in which we calculate GCC, one capturing the grass layer (`gcc_gr`) and one
178 capturing the trees (`gcc_tr`). The data derived from RGB images can be found on the website of the PhenoCam network (IDs:
179 ES-LM1, ES_LMa and ES_LM2 for the NT, CT and NPT, respectively). At each site we chose the masks GR_1000 for the
180 grass layer and EB_1000 for the trees.

181
182 We further calculated albedo as the ratio of outgoing shortwave radiation to incoming shortwave radiation, measured at the
183 radiometric tower setup at each site. We distinguished ecosystem albedo (`Alb_eco`), tree (`Alb_tr`) and grass albedo (`Alb_gr`) to
184 account for reflectance and as another proxy for vegetation greenness and water status of the plants. We used daily averages
185 from only daytime hours (11:00-15:00) to guarantee a high solar zenith angle for reliable measurements. Furthermore, cloudy
186 days were filtered out and only timesteps where the ratio of downward radiation to extra-terrestrial radiation at the top of the
187 atmosphere was 0.7 or more were kept (Wood et al., 2015).

188
189 Finally, we use Normalized Difference Vegetation Index (NDVI) from the FluxnetEO dataset, as a proxy describing the amount
190 and health of vegetation cover (Tucker, 1979). The dataset complements ground measurements by providing satellite-based
191 vegetation indices, surface reflectance and land surface temperatures for a 2 km radius around a flux site (Walther et al., 2022).
192 We use NDVI from MODIS (Moderate Resolution Imaging Spectroradiometer) with a daily temporal resolution (Walther et
193 al., 2022). NDVI is calculated from the normalized difference between the reflectance of near-infrared (NIR) and red-light
194 bands (Tucker, 1979).



195

196

197

198

Table 1: Flux, meteorological, soil variables and vegetation indices used in this study. Soil heat flux and soil temperatures were calculated based on the shadow fraction estimated from the solar zenith angle (variable SZA) and a canopy cover of 20%.

variable name	variable description	unit	measurement device	measurement height/depth
NEE	net ecosystem exchange on ecosystem level	$\mu\text{mol m}^{-2} \text{s}^{-1}$	R3-50, Gill LTD UK, LI-7200	15m, 15.5m (CT)
EF	evaporative fraction		R3-50, Gill LTD UK, LI-7200, calculated	15m, 15.5m (CT)
air_press	air pressure	Pa	Young 61302V	
Rh02	relative humidity at 2m	%	CPK1-5	2m
Rh15	relative humidity at 15m	%	CPK1-5	15m
Ta02	temperature at 2m	degreeC	CPK1-5	2m
Ta15	temperature at 15m	degreeC	CPK1-5	15m
VPD	water vapor pressure deficit	Pa	calculated	15m
ustar	friction velocity	m s^{-1}	R3-50, Gill LTD UK	15m
SWDR	short wave downward radiation	W m^{-2}	CMP22/CNR4	9m
LWDR	long wave downward radiation	W m^{-2}	CNR4	9m
PAR	incoming photosynthetically active radiation	$\mu\text{mol m}^{-2}$	Kipp& Zonen PQS1	9m
SWCn	normalized soil moisture content for top 20cm		ML2x, Delat-T Devices Ltd	20cm
SHF_Sun	soil heat flux sun	W m^{-2}	HP3/CN3 Rimco	5cm
SHF_Shadow	soil heat flux shadow	W m^{-2}	HP3/CN3 Rimco	5cm
T _{soilSun}	soil temperature sun	degree C	UMS Th3-s	10 cm
T _{soilShadow}	soil temperature shadow	degree C	UMS Th3-s	10 cm
Alb_eco	ecosystem Albedo		CNR4	15 m
Alb_gr	grass level Albedo		CNR4	9m (CT, NT), 12m (NPT)
Alb_tr	tree level Albedo		CNR4	9m (CT, NT), 12m (NPT)
gcc_gr	grass level green chromatic coordinates		stardot netcam SC5	15m
gcc_tr	tree level green chromatic coordinates		stardot netcam SC5	15m
NDVI	normalized difference vegetation index		MODIS satellite	

199



200

201 **2.4 Data Analysis**

202 **2.4.1. Aggregation to daily data**

203 For our analysis we calculated from the biometeorological and flux data daily mean values aggregated from the half-hourly
204 measured values during daytime. Daytime includes only values measured after sunrise and before sunset, identified using the
205 *suncalc* package in R (Thieurmel, 2017). We discarded flux measurements with quality flag 1-3 and kept only measured values
206 to not confound following analyses of NEE controls with gap-filled values which are based on other meteorological variables.
207 This does not apply to vegetation indices as they were calculated as described above. GPP and R_{eco} were not assessed in this
208 study as partitioning methods depend on other environmental factors that would also confound the analysis of NEE controls.
209 If not stated differently, the following analyses cover the 7-year period from 2016-2022 as in this time all variables are available.
210 For the assessment of NEE variability and budgets, we utilized data spanning 8 years (2016-2023) because this extended
211 dataset was available and incorporating additional years enhances the robustness of observed trends.

212 **2.4.2 Time Series Decomposition with Singular Spectrum Analysis**

213 Decomposition methods assume that observed time series are composed of additively superimposed sub-signals, each shaped
214 by different scales of variability (Mahecha et al., 2010). Consequently, the time series represents the sum of a trend, oscillatory
215 components at various scales, and noise (Liu et al., 2022).

216 Here we used Singular Spectrum Analysis (SSA) for the decomposition. SSA is entirely data-driven and non-parametric and
217 is therefore free of the bias of function-selection (Golyandina et al., 2001; Liu et al., 2022; Mahecha et al., 2007). This makes
218 it advantageous compared to other decomposition methods like Fourier and wavelet analysis (Baldocchi et al., 2021). It is
219 more flexible in grouping components of similar frequencies than wavelet decomposition (Liu et al., 2022) and able to detect
220 aperiodic or non-harmonic sub-signals from short and noisy signals (Golyandina and Zhigljavsky, 2013; Mahecha et al., 2007).
221 Since it is fully phase-amplitude modulated, and relatively robust against instationarities of the signal mean and variance, it is
222 suitable for nonstationary signals (Allen and Smith, 1996; Golyandina and Zhigljavsky, 2013; Yiou et al., 2000). Even
223 fragmented timeseries can be handled with it, as SSA can be used for filling gaps according to the first reconstructed component
224 which is a low-frequency signal (Kondrashov and Ghil, 2006). This makes it particularly useful for flux data (Mahecha et al.,
225 2007).

226 SSA consists of four steps: embedding, decomposition, grouping and reconstruction. In the first step a one-dimensional
227 timeseries $y(t)$ is embedded into a two-dimensional lagged matrix X , by shifting a moving window of a certain window length
228 (L) along the timeseries. In the second step X is decomposed into its orthogonal components by determining eigenvalues and
229 eigenvectors corresponding to principal components (singular value decomposition). Then the eigenvalues of the covariance
230 matrix $X \cdot X$ are ranked. In the next step, the components are grouped, as some sub-signals consist of a set of components with



231 complementary oscillatory frequency. In the last step, by inverting the ranked principal components, the reconstructed
232 components of the original time series are computed. These reconstructed components show how much of the variability of
233 the original timeseries is associated with the different timescales. A more detailed description of the method can be found in
234 Golyandina et al. (2018).

235 Here we used the rssa – package in R (Golyandina and Korobeynikov, 2014) for our analysis. To support our hypothesis that
236 daily-scale NEE variations are predominantly influenced by radiation, with a neglectable effect of nutrient addition, we
237 conducted a preliminary analysis extracting the daily signal of NEE and all potential driving variables from half-hourly
238 measurements. Detailed procedures and results of this analysis are provided in the Supplementary Material (S1).

239 For our analysis we extracted the seasonal signal of the daily timeseries of all variables shown in Table 1. First, we gap-filled
240 the timeseries with the igapfill – function. For gap-filling, as a window length (L) of $n/2.5$ is recommended (Mahecha et al.,
241 2007), we selected a gap-filling window length of $L = 1000$ for 2557 datapoints from 7 years of daily data. By conducting a
242 sensitivity analysis, we found that adding a three-month margin at the beginning and the end of a timeseries can help to reduce
243 edge effects during the gap-filling (details see S.2).

244 To extract the seasonal signal, we reconstructed the components of the frequency bin of 15 to 366 (days). We selected $L = 732$
245 (2 years) based on the criteria that L should be less than $n/2$ and ideally an integer multiple of the period length to be extracted
246 to ensure a clear signal (Biriukova et al., 2021; Golyandina and Zhigljavsky, 2013). Frequency contributions of less than 0.2
247 were defined as noise (Liu et al., 2022). For the grouping we used the automated method provided by the rssa-package, which
248 identifies groups using a hierarchical clustering algorithm based on the w-correlation matrix. The w-correlation matrix shows
249 the weighted correlations between reconstructed components (Buttler, 2014; Golyandina and Korobeynikov, 2014).

250 For analysing the changes in seasonal NEE variability and budgets, we used data from 2016-2023. Accordingly, L was set at
251 1169 ($L = n/2.5$, with $n = 3105$). To account for seasonal variability, we calculated for each year the standard deviation of the
252 reconstructed NEE signal to capture the variation amplitude.

253 2.4.3 Pearson Correlation Coefficient

254 To find out the key drivers of NEE we first computed in R the Pearson correlation coefficients (r) between NEE and all the
255 investigated variables (Table 1) from the reconstructed seasonal signal using the daily datasets. It is calculated as follows:

$$256 \quad r = \frac{\sum_{i=1}^n (x_i - \underline{x})(y_i - \underline{y})}{\sqrt{\sum_{i=1}^n (x_i - \underline{x})^2 \sum_{i=1}^n (y_i - \underline{y})^2}} \quad (2)$$

257
258 With n as the timeseries length, x_i and y_i as the single timestep values within the timeseries and \underline{x} and \underline{y} as the sample means.
259 We calculated values for each tower and then ranked r according to their absolute value to identify the main drivers of NEE.



260 2.4.4 Information Theory

261 To consider collinear relationships and potential lagging effects between NEE and its controls, we extended our analysis using
262 information theory. Metrics of Mutual Information (MI) are a powerful tool to understand non-linear and feedback-driven
263 relationships in complex ecosystems (Chamberlain et al., 2020; Knox et al., 2018). MI is a non-parametric method and can
264 disentangle interactions on different scales (Chamberlain et al., 2018; Knox et al., 2018; Sturtevant et al., 2016), by describing
265 the average tendency for joint states of two variables X and Y to co-occur (Fraser and Swinney, 1986). This means it quantifies
266 the amount of information that two variables X and Y hold in common, or the reduction of uncertainty of one variable, given
267 the knowledge of the other (Chamberlain et al., 2020; Knox et al., 2021). It is a normalized measure of the statistical
268 dependence of Y on X and no prior knowledge about their relationship is needed (Liu et al., 2022). Larger values indicate
269 higher dependence, or a stronger interaction between the variables. With Shannon entropy (H_x) we can quantify the uncertainty
270 in a system:

$$272 H_x = -\sum_{x_t} p(x_t) \log_2 p(x_t) \quad (3)$$

274 with $p(x)$ as the marginal probability distribution of X, and X_t as the different states of X in the timeseries t. Here we discretized
275 the states of continuous variables into ten fixed-interval histogram bins, as Sturtevant et al. (2016) and Ruddell and Kumar
276 (2009) showed that ten histogram bins ensure sufficient resolution for a robust estimate. MI then was calculated with both the
277 marginal and joint probability distributions of X and Y, $p(x,y)$:

$$279 MI = \sum_{x_t} p(x_t, y_t) \log_2 \frac{p(x_t, y_t)}{p(x_t)p(y_t)} \quad (4)$$

281 To make the MI between NEE and different potential drivers comparable, we used here a normalized form of MI:

$$283 MI_{sync} = \frac{MI}{H_y} \quad (5)$$

284 We refer to this relative MI as synchronous MI (MI_{sync}), as it depicts the interaction between X and Y at the concurrent time
285 step. A further power of MI lies in its capability to account for the temporal direction (τ) of the interaction between X and Y
286 (Liu et al., 2022):

$$289 MI_{max} = MI_{sync(\tau)} = \frac{\sum_{x_{t-\tau}} \sum_{y_t} p(x_{t-\tau}, y_t) \frac{p(x_{t-\tau}, y_t)}{p(x_{t-\tau})p(y_t)}}{-\sum_{y_t} p(y_t)p(y_i)} \quad (6)$$



290

291 Positive and negative values of τ show an asynchronous interaction between X and Y, with a lag or lead in Y relative to X. We
292 chose 60 days as maximum value for τ to check if the potential driving variable (Y) is leading NEE (X) or vice versa (Liu et
293 al., 2022). We then picked the highest MI value (MI_{\max}) in this window and the respective day of its occurrence. If $MI_{\text{sync}} >$
294 MI_{\max} , the interaction is synchronous, if $MI_{\text{sync}} < MI_{\max}$, the interaction is asynchronous. If $\tau < 0$, Y lags X, if $\tau > 0$, Y leads X
295 and can therefore be characterized as a driver or control of X. Significance thresholds were calculated from the 95th percentile
296 ($p < 0.05$) of 1000 Monte Carlo random walks of the independent variable (Chamberlain et al., 2020; Ruddell and Kumar,
297 2009). We calculated MI measures and the confidence thresholds in R, based on functions by Chamberlain et al. (2020).

298 We determined MI_{sync} and MI_{\max} for the 7-year time series (2016-2022) from the reconstructed seasonal signal. Gap-filled
299 timesteps by SSA were removed before both the calculation of r and MI measures. Only for NDVI we kept them, as the gap-
300 filling is based on the original timeseries and does not depend on other variables (Walther et al., 2022). It therefore does not
301 confound the analysis of potential drivers.

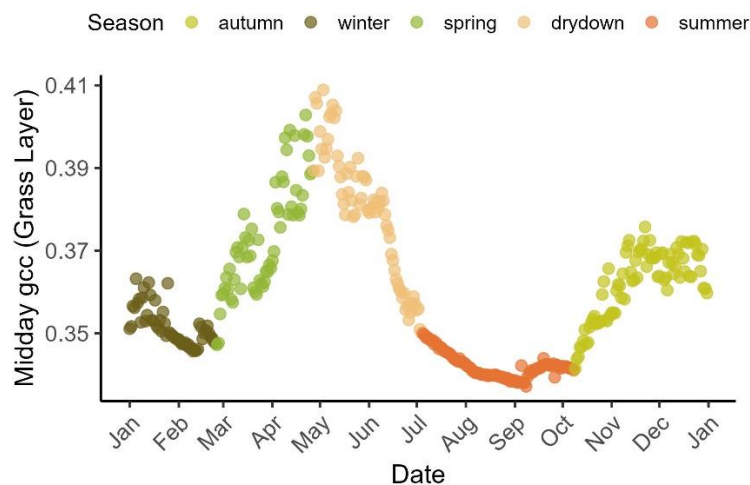
302

303 2.4.5 Phenological Seasons

304 As the NEE controls vary in their importance in different seasons (Baldocchi and Arias Ortiz, 2024), we calculated MI_{sync} for
305 each season to better capture how the nutrient addition and stoichiometric balance change the importance of different drivers
306 over the study period. As this ecosystem's strong seasonality is reflected in vegetation activity, we assigned seasons using
307 PhenoCam imagery. We defined phenological seasons following Nair et al. (2024). Phenological transition dates were
308 extracted using GCC at all three sites according to changes between stationary and rising or declining greenness (Luo et al.,
309 2018). Then, phenological transition dates averaged across the three sites for each year were calculated. According to these
310 dates, each day of the 7-year timeseries was assigned to one season, describing different phases of net vegetation activity (i.e.,
311 spring, drydown, summer, autumn and winter, as described above in Chapter 2.1.). Figure 1 illustrates a typical annual cycle
312 of the seasons at Majadas de Tiétar.

313 We calculated MI_{sync} values for each pair of interest (NEE and potential driving variable) in each season across all 7 years
314 together. In addition, we estimated yearly MI_{sync} for each single season (35 datapoints) to evaluate how sensitivity of NEE to
315 drivers developed over time. To isolate the fertilization effect on the importance of different drivers for NEE, we calculated
316 the differences in the MI_{sync} values of each season in each year between the fertilized plots and the control plot, i.e., NT – CT
317 and NPT – CT, referred to as MI_{diff} . We plotted the MI_{diff} values for each season along the 7-year period and calculated linear
318 regressions to confirm whether there are significant trends in the importance of drivers. The significance level was set at $p <$
319 0.05. Variables with $MI_{\max} < 0.2$ were discarded.

320



321

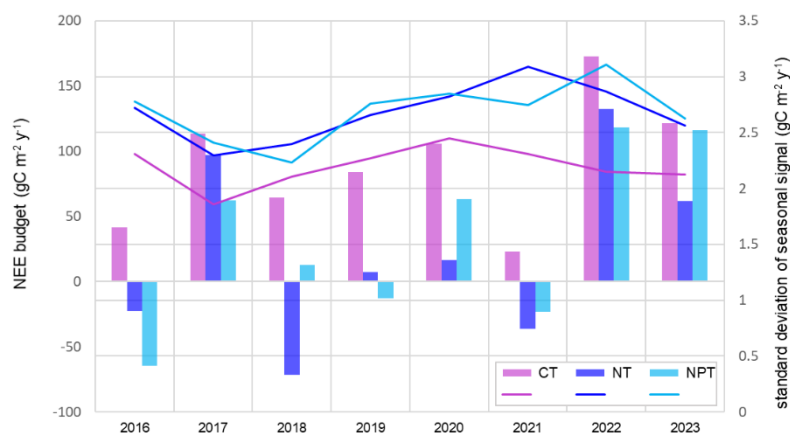
322 **Figure 1: A typical annual cycle of midday green chromatic coordinates (gcc) derived from the grass layer at the control plot in**
 323 **2018, showing the five phenological seasons – winter, spring, drydown, summer and autumn. Spring is the main growing season**
 324 **(first peak in May), the grasses become senescent during drydown and dormant in summer, regreening starts (second peak around**
 325 **November) in autumn with the onset of rains, and winter is radiation and temperature limited.**

326 3 Results

327 3.1 Seasonal NEE Variability

328 At CT, not experiencing any manipulation, the annual ecosystem NEE derived from EC measurements was positive for the
 329 2016-2023 period, with an average annual NEE budget of $90.8 \pm 48.0 \text{ gC m}^{-2} \text{ y}^{-1}$. This indicates that the ecosystem acted as a
 330 CO_2 source. With fertilization treatment, the measured ecosystem NEE shifted towards CO_2 neutrality, with annual averages
 331 of $34.1 \pm 66.7 \text{ gC m}^{-2} \text{ y}^{-1}$ and $23.1 \pm 69.5 \text{ gC m}^{-2} \text{ y}^{-1}$ at NPT and NT, respectively. Annual NEE budgets fluctuated between
 332 positive and negative values at the fertilized plots, while CT consistently showed positive NEE throughout the years. In the
 333 years of 2017, 2022 and 2023, we observed high positive NEE values (i.e., stronger CO_2 source) at all three plots. Conversely,
 334 in years such as 2016, 2018, and 2021, fertilized areas exhibited higher CO_2 uptake, acting as stronger CO_2 sinks (Fig.2). This
 335 illustrates the high interannual variability of the CO_2 fluxes in this ecosystem and the substantial impact of fertilization.
 336 Additionally, the nutrient addition led to higher seasonal variability of NEE, as shown by the greater yearly standard deviation
 337 of the seasonal reconstructed signal. The variability at NT and NPT further exhibited an increasing pattern over time (Fig.2).
 338 In 2017, NEE had comparatively low seasonal variability at all three sites, which might be attributed to the extraordinary
 339 dryness in that year.

340



341

342

343

344

Figure 2: Annual net ecosystem exchange (NEE) budgets ($\text{gC m}^{-2} \text{y}^{-1}$) and yearly standard deviations calculated using the seasonal reconstructed signals at the three sites for the 2016-2023 period. CT- control site, NT – nitrogen fertilized site, NPT – nitrogen and phosphorus fertilized site.

345

346 3.2 Key NEE controls

347

348

349

350

351

352

353

354

355

356

357

358

359

360

361

362

363

364

We identified key controls of NEE at the three plots, comparing the results of Pearson correlation coefficient r , which considers only linear relationships between variables, and with Mutual Information (MI), which accounts for collinear relationships. and MI_{sync} and r values show synchronous relationships, MI_{max} values can account for leading and lagging interactions by identifying the day of the highest interaction between the potential driver and NEE within a 60-day window.

At all plots, gcc_{gr} (i.e., grass layer GCC) and NDVI (at ecosystem level) were the most important predictors of NEE (Fig. 3). Both r and MI identified these proxies representing vegetation greenness as the most significant drivers. They were followed by EF (i.e., the fraction of heat transport that is done by LE), which is influenced by meteorological variables (such as soil moisture, net radiation and VPD) as well as vegetation properties like LAI.

Regarding micrometeorological variables, at CT, T_{soilShd} and T_{a15} exhibited strong interactions with NEE using both r and MI_{sync} . Using r , LWDR, and SWCn were also important in explaining NEE variations, while MI_{sync} indicated that T_{a02} and T_{soilSun} were more significant (Fig.3 (a), (b)). Variables describing water availability, such as VPD, SWCn and Rh were ranked in the middle ranges by MI_{sync} (e.g., VPD at rank 9 and SWCn at rank 14). The MI analysis provided deeper insights into the interactions between the environment and NEE by considering leading and lagging effects, as shown by MI_{max} (Fig. 3(c)). NDVI showed the highest interaction with NEE at a time lag of 16 days, and the second most important driver, gcc_{gr} , had a lag of 7 days. When considering leading and lagging effects, EF became relatively less important with a value of 0.29 at 15 days. Soil temperatures were identified amongst the five most important controls by MI_{max} , with lags of 37 and 43 days for T_{soilShd} and T_{soilSun} , respectively. SWCn was also important (ranked 6th) with a 20-day lag. Other variables such as air temperature and VPD showed the highest interaction with a lag of around a month. Radiation-related variables like PAR and

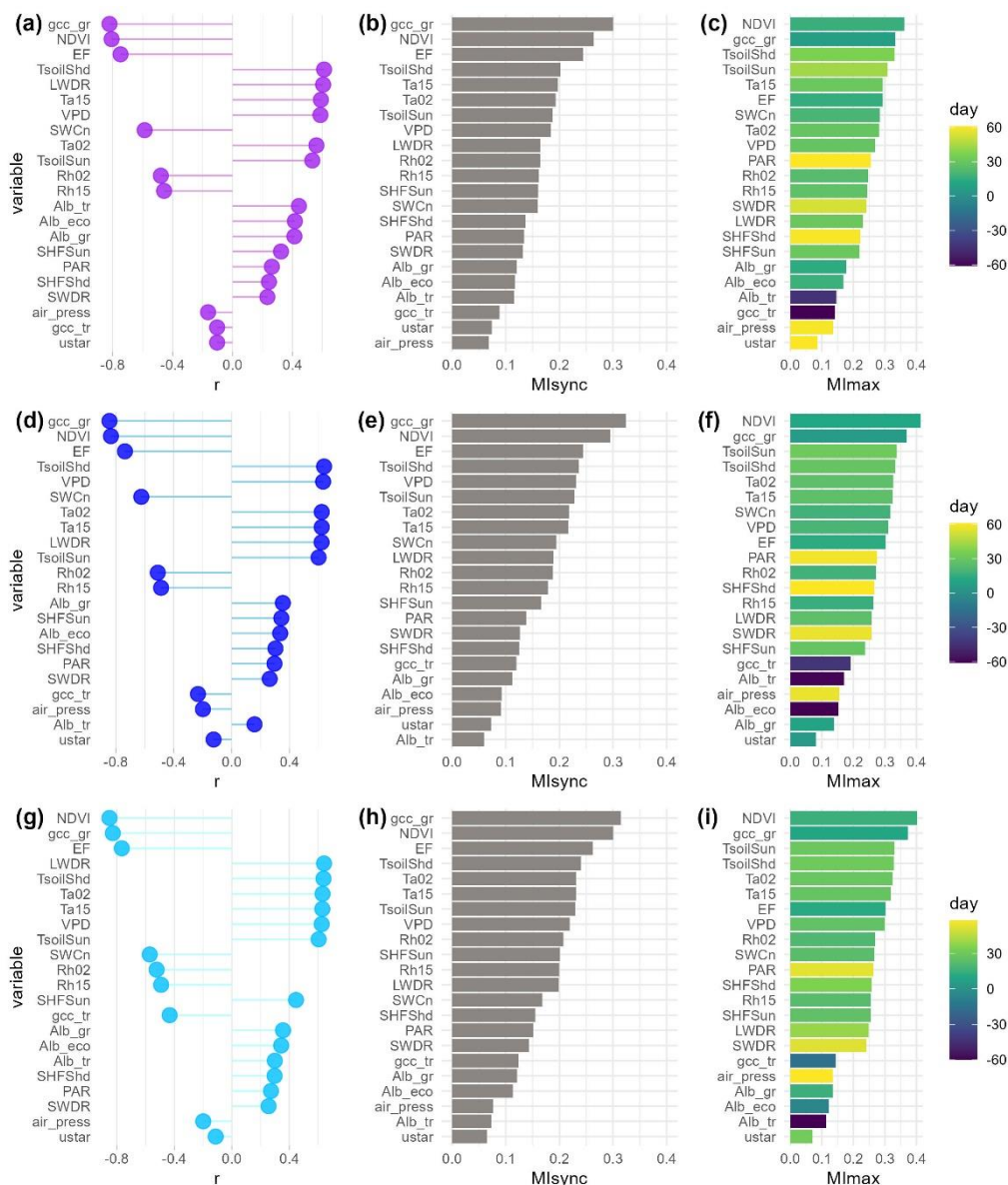


365 SWDR exhibited long lag times in their highest interaction with NEE (60 days and 53 days, respectively). All MI values can
366 be found in the Supplementary Material (S3).

367 At NT, the two synchronous methods agreed on the twelve most important predictors, with the exception that MI_{sync} identified
368 SWCn and LWDR as less important and $T_{soilSun}$ as more important compared to r (Fig.3 (d), (e)). Soil temperatures, VPD,
369 SWCn and air temperatures were among the most significant controls, following the most important drivers, vegetation
370 greenness and EF. NDVI showed the highest interaction with NEE with a lag of 12 days, followed by gcc_gr with a lag of 6
371 days. Soil temperatures exhibited the highest interactions with a lag of around a month, while air temperatures showed the
372 highest interaction at a lag of 26 days. Moisture-related variables all showed similar time lags, with relative humidity having
373 the highest interaction with NEE at 16-18 days prior, similar to SWCn and VPD at 18 and 20 days, respectively. EF had the
374 highest interaction with NEE at a lag of two weeks. Shortwave radiation-related variables showed a strongly lagged effect (i.e.,
375 PAR 59 days, SWDR 57 days), while the effect of longwave radiation LWDR is less lagged, showing the strongest interaction
376 26 days prior (Fig.3 (f)).

377 At NPT, both r and MI_{sync} detected soil temperatures, air temperatures and VPD as the most important NEE controls behind
378 gcc_gr and NDVI, with only minor differences. LWDR was more important using r compared to MI_{sync} . SWCn and Rh were
379 in the middle ranks, PAR and SWDR in the lower ranks (Fig.3 (g), (h)). Additionally, NDVI and gcc_gr led NEE with the
380 strongest interaction at lags of 2 weeks and 10 days, respectively, followed by soil temperatures and air temperatures with the
381 highest interaction at a lag of around a month (Fig.3 (i)). EF showed the highest interaction at a lag of 12 days. Other moisture-
382 related variables like VPD, SWCn, and Rh were also detected to be in the middle ranks by MI_{max} , with time lags of 26, 23, and
383 20 days, respectively. PAR and SWDR showed the highest interaction with NEE at time lags of 53 and 52 days, respectively
384 (Fig.3 (i)).

385 MI and r agreed in the detection of the most important drivers, thereby proving that information theory is applicable to our
386 case. Therefore, in the remainder of this paper we focus on values obtained using MI, as MI is able to detect collinear
387 relationships as well as leading and lagging effects. Additionally, we discuss variables with $MI_{max} > 0.2$ in the following
388 sections to concentrate on the information provided by variables with greater explanatory value.



389

390

391

392

393

394

Figure 3: Pearson correlation coefficient (r) (a), (d), (g), synchronous mutual information (MI_{sync}) (b), (e), (h) and maximum mutual information within a 60-day window (MI_{max}) (c), (f), (i) between net ecosystem exchange (NEE) and potential drivers over the 7-year period (2016-2022) at the control plot CT (a)-(c), the nitrogen fertilized plot NT (d)-(f) and the nitrogen and phosphorus fertilized plot NPT (g)-(i). The color scale in the MI_{max} plots indicates the day when MI_{max} occurs, positive values indicate that the variable leads NEE, negative values vice versa.

395



396 3.3 Effect of Fertilization on NEE Sensitivity to its Controls

397 The relationships between NEE and biogenic and environmental variables were asynchronous, as indicated by $MI_{sync} < MI_{max}$
398 for all variables. Therefore, we focused on MI_{max} to describe the differences in NEE sensitivity to various controls across
399 towers.

400 At NT and NPT, NDVI showed a slightly higher interaction with NEE (0.41 and 0.40) than at CT (0.36). However, the time
401 lag was smallest at NT (12 days) compared to 15 and 16 days at NPT and CT, respectively. Thus, N fertilization appeared to
402 shorten the reaction time of NEE to changes in NDVI. GCC at the grass level showed higher explanatory value for NEE at
403 NPT and NT ($MI_{max} = 0.37$) compared to CT ($MI_{max} = 0.33$). EF showed only slight differences in interaction strengths among
404 the sites. At CT, MI_{max} was 0.29 with a lag of 15 days, MI_{max} were 0.30 with lag times of 14 and 12 days at both NT and NPT,
405 respectively (Fig. 4, S3).

406 Relative humidity at two heights showed the lowest interaction with NEE at CT with MI_{max} values around 0.24, while the
407 fertilized sites had slightly higher values of 0.26-0.27. Furthermore, the reaction time of NEE to relative humidity decreased
408 with fertilization. At CT, the time lag was 24-27 days, at NPT it was 20-22 days and at NT 16-18 days. VPD showed the
409 highest explanatory value for NEE at NT ($MI_{max} = 0.31$), followed by NPT ($MI_{max} = 0.30$) and CT ($MI_{max} = 0.27$). The
410 interaction between NEE and air temperatures was slightly higher at the fertilized plots compared to the control. The MI_{max}
411 value was around 0.28 at CT, but higher at around 0.32 at NT and NPT. Soil temperatures showed similar interaction strength
412 with NEE across treatments, with MI_{max} ranging from 0.31 to 0.33 (Fig. 4, S3).

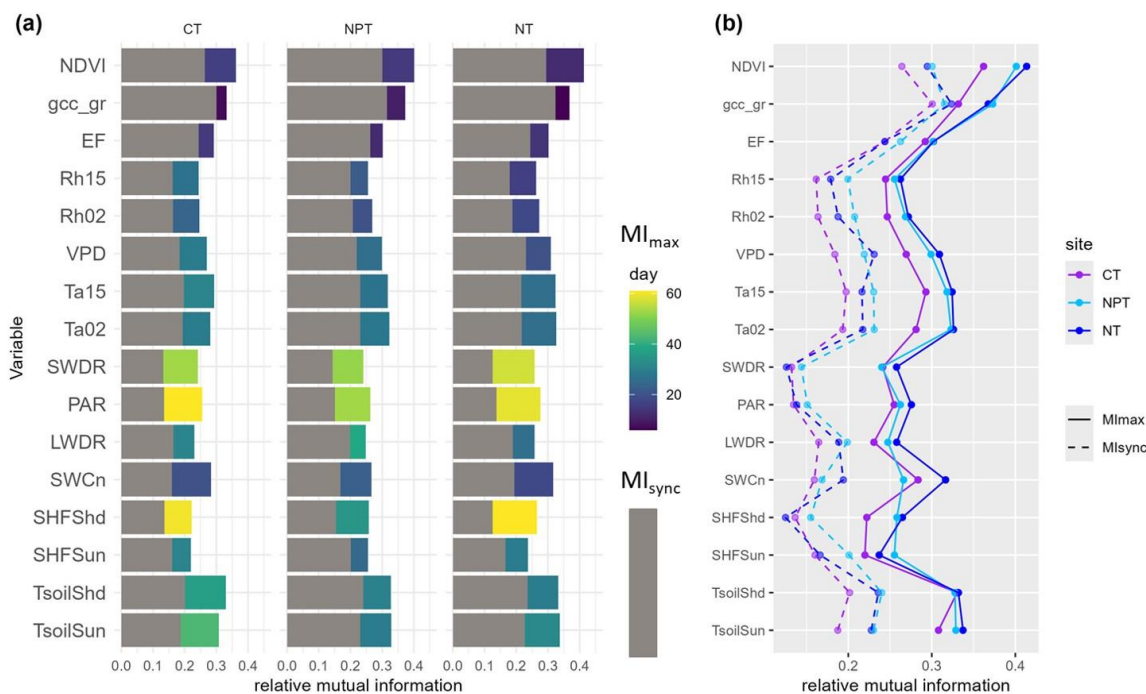
413 Regarding radiation variables, PAR showed slightly higher interaction with NEE at NT ($MI_{max} = 0.28$), than at NPT ($MI_{max} =$
414 0.26) and CT ($MI_{max} = 0.25$). Similarly, SWDR showed highest interaction with NEE at NT ($MI_{max} = 0.26$), while at NPT and
415 CT it was equally strong ($MI_{max} = 0.24$).

416 In terms of soil variables, soil temperatures exhibited the strongest interaction with NEE. While soil temperatures below the
417 canopy ($T_{soilShd}$) were almost the same across sites ($MI_{max} = 0.33$), the importance of soil temperatures under open air differed
418 at CT ($MI_{max} = 0.31$) compared to the fertilized plots (0.34 and 0.33 at NT and NPT, respectively). SWCn showed the highest
419 explanatory value for NEE at NT ($MI_{max} = 0.31$), followed by CT ($MI_{max} = 0.28$) and NPT ($MI_{max} = 0.27$) (Fig. 4, S3).

420 An overview plot with all variables including the ones with $MI_{max} < 0.2$ is provided in the Supplementary Material (S4).

421

422 Nutrient addition did not show a substantial effect on the sensitivity of ecosystem NEE to different drivers over the 7-year
423 scale when considering the whole time series together. In the next step we examined the different seasons in greater detail.



424

425 **Figure 4: (a) Synchronous (MI_{sync} , grey) and maximum (MI_{max} , colours) mutual information at the control site (CT), the nitrogen**
 426 **fertilized site (NT) and the nitrogen and phosphorus fertilized site (NPT) at the seasonal scale. The colour scale indicates the day**
 427 **when MI_{max} occurs, with positive values indicating that the variable leads net ecosystem exchange (NEE) and vice versa. (b) MI_{sync}**
 428 **(dotted lines) and MI_{max} (solid lines) values at the three sites. Variables with $MI_{max} < 0.2$ are not shown here.**

429

430 3.4 Identifying Driver Importance in Different Phenological Seasons

431 We split the 7-year dataset into five different phenological seasons derived from grass layer GCC derived from PhenoCam
 432 photos, and calculated MI_{sync} between NEE and each of the drivers. This analysis showed that the most important drivers
 433 differed between seasons and treatments (Table 2).

434 In the winter, the water vapor transfers of available energy, represented by EF, show a strong interaction with NEE at NPT
 435 and CT. Further, NDVI and tree-layer albedo, as well as radiation parameters such as PAR and SWDR were important in
 436 explaining NEE variations.

437 In the spring (i.e., the main growing season), NDVI and GCC at grass (gcc_{gr}) and tree (gcc_{tr}) levels showed the strongest
 438 interactions with NEE, indicating that NEE was dominated by photosynthetic activity (GPP) during this season. Furthermore,
 439 soil temperatures showed strong interactions with NEE at CT and NPT, but not at NT.

440 During the drydown phase, NEE was dominated by NDVI across treatments, with GCC at the grass level (gcc_{gr}) also showing
 441 strong interactions with NEE at CT and NPT. At NT, VPD exhibited a strong link with NEE, which was not as dominant at
 442 the other plots.



443 In the summer, soil temperatures showed high interactions with NEE, possibly relating to soil respiration. Additionally,
 444 radiation parameters (i.e., SWDR, PAR) were important in explaining NEE variations during this season. At CT and NT, tree-
 445 layer GCC became important, which was logical as the grass layer becomes senescent in the summer and is dormant in terms
 446 of the ecosystem carbon flux. At NPT, gcc_gr showed a higher interaction with ecosystem NEE than gcc_tr.
 447 In autumn, the regreening starts with the onset of rains, and NDVI and grass layer GCC (gcc_gr) showed strong interactions
 448 with NEE, as GPP starts to dominate NEE again, driven by photosynthetic activity. Additionally, soil temperatures had a strong
 449 link with NEE (as soil respiration is also high in this season), strongest at CT, as well as air temperatures.

450

451 **Table 2: Five most important drivers in each phenological season at each tower derived using synchronous mutual information. CT**
 452 **= control site, NT = nitrogen fertilized site, NPT = nitrogen + phosphorus fertilized site.**

	CT	NT	NPT
Winter wet and energy limited	1. Alb_tr	PAR	EF
	2. PAR	Alb_tr	NDVI
	3. EF	SWDR	PAR
	4. T _{soilShd}	NDVI	SWDR
	5. T _{soilSun}	SHF_Sun	T _{soilSun}
Spring main growing season	1. gcc_gr	NDVI	NDVI
	2. NDVI	gcc_tr	gcc_gr
	3. gcc_tr	gcc_gr	gcc_tr
	4. T _{soilSun}	Alb_tr	T _{soilSun}
	5. T _{soilShd}	EF	T _{soilShd}
Drydown senescence of grass layer	1. NDVI	NDVI	NDVI
	2. T _{soilShd}	T _{soilSun}	gcc_gr
	3. gcc_gr	T _{soilShd}	T _{soilShd}
	4. EF	VPD	T _{soilSun}
	5. T _{soilSun}	EF	EF
Summer Dormant/dead grass layer	1. PAR	SHF_Shhd	T _{soilSun}
	2. T _{soilSun}	PAR	T _{soilShd}
	3. SHF_Shhd	SWDR	SHF_Sun
	4. gcc_tr	gcc_tr	gcc_gr
	5. SHF_Sun	NDVI	PAR
Autumn Regreening of grass layer with onset of rains	1. T _{soilShd}	NDVI	NDVI
	2. gcc_gr	gcc_gr	gcc_gr
	3. NDVI	T _{soilShd}	T _{soilShd}
	4. Ta15	Ta02	T _{soilSun}
	5. T _{soilSun}	Ta15	Ta15

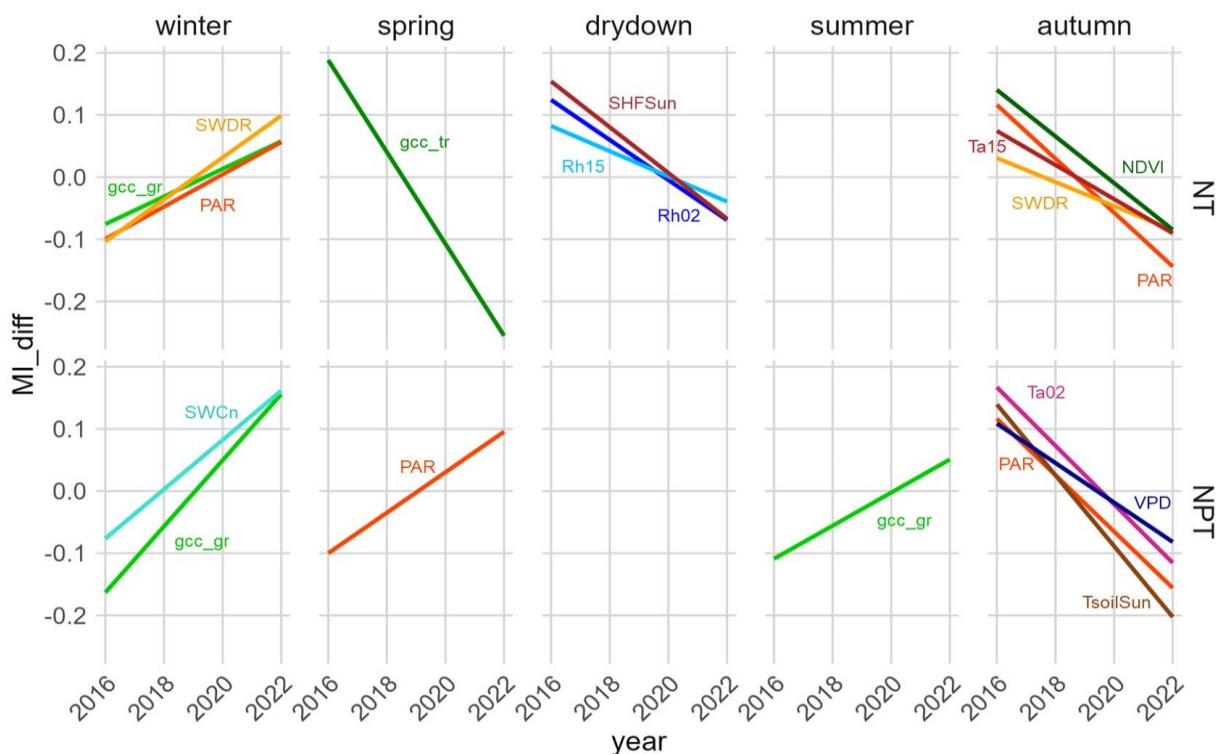


453

454 **3.5 Changes in NEE Sensitivity over Time**

455 We observed that with N addition, NEE became less sensitive to certain variables during autumn (i.e., the regreening phase),
 456 the drydown phase, and winter over time (Fig.5). Specifically, in autumn, the sensitivity of ecosystem NEE to changes in air
 457 temperature (Ta15), shortwave radiation (SWDR and PAR), and NDVI decreased significantly over the 7-year period. In the
 458 drydown phase, the sensitivity of ecosystem NEE to changes in relative humidity (Rh02 and Rh15) and soil heat flux (SHF_Sun)
 459 also decreased significantly. In winter, however, we observed a significant increase in the sensitivity of NEE to variations in
 460 PAR, SWDR, and grass layer GCC (gcc_gr).

461 With the addition of N+P, significant changes in NEE sensitivity over time were observed in all seasons except the drydown
 462 phase (Fig.5). In autumn, the fertilization with N and P led to a significant decrease in NEE sensitivity to air and soil
 463 temperatures (Ta02 and T_{soilSun}), PAR, and VPD. In spring, which is the main growing season, NEE sensitivity to variations
 464 in PAR increased significantly over time. In summer, NEE became significantly more sensitive to changes in grass layer GCC.
 465 In winter, NEE shows a significant increase in sensitivity to changes in both grass layer GCC (gcc_gr) and soil water content
 466 (SWCn).



467

468 **Figure 5: Linear regressions of the seasonal synchronous mutual information difference (MI_{diff}) between NT and CT (bottom) and**
 469 **between NPT and CT (top) in different phenological seasons. Only the relationships with significant trends are shown. Significance**
 470 **level is set at $p < 0.05$. Variables with overall $MI < 0.2$ at all towers are not shown here.**



471 **4 Discussion**

472 **4.1 Nutrient addition increases seasonal NEE variability, driven by grass layer**

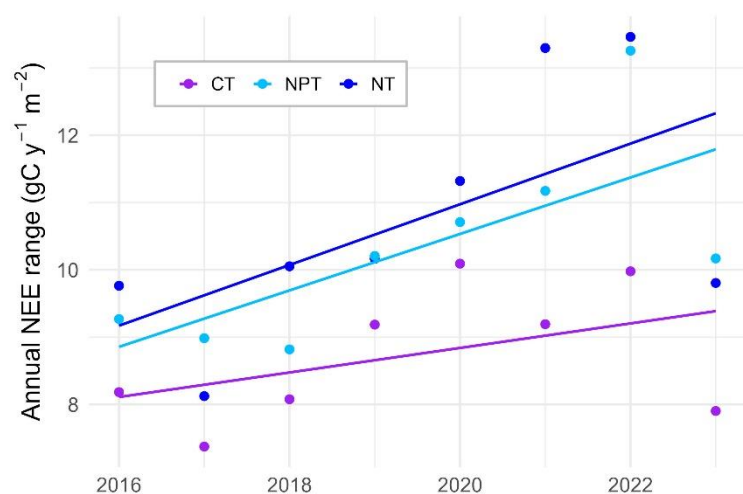
473 Our results indicate that nutrient addition enhances seasonal NEE variability compared to the control. Additionally, the
474 seasonal variability increases over time at the fertilized plots. Looking at the difference between annual NEE maximum and
475 annual NEE minimum, we notice a significantly increasing trend at the NPT plot (Fig.6). We argue that this nutrient effect is
476 dominated by grass layer which substantially controls the NEE dynamics in this system. Our analysis supports that grass layer
477 GCC and NDVI are most important in explaining NEE variations across treatments (Fig. 3, 4). Both variables represent grass
478 layer greenness, as the larger fraction of the surface consists of annual grasses (Bogdanovich et al., 2021) and remotely sensed
479 NDVI is dominated by the herbaceous layer.

480

481 The added nutrients mostly stay in the herbaceous layer at the study sites (El-Madany et al., 2021), and it is therefore more
482 affected by the nutrient manipulation than trees. It has been found that the nutrient addition leads to higher root biomass and
483 root length density (Nair et al., 2019) and N can be absorbed and used for leaves. In the leaves, N enhances the photosynthetic
484 capacity (Fleischer et al., 2013) which supports the faster increase in maximum GPP and biomass in the fertilized plots, as
485 confirmed by Luo et al. (2020). NT and NPT show higher productivity and therefore higher biomass amount compared to the
486 control (Luo et al., 2020). As the grass layer is senescent in summer, this results in a higher amount of dead biomass, which
487 will then be respired by soil microbes (Manzoni et al., 2020; Moyano et al., 2013) as soon as there is sufficient water available
488 (Huxman et al., 2004). This indicates that there is a higher carbon turnover at the fertilized plots, leading to an increased range
489 of NEE within a year (Fig.6). It agrees with findings from Ma et al. (2016), who found in a Californian oak grass savanna that
490 the amount of grass litter determines the size of the fast carbon pool in consecutive seasons.

491 Evergreen tree species have relatively constant foliage amount throughout the year and are able to use their deeper roots to
492 access lower water resources in the soil (Baldocchi et al., 2004; Rolo and Moreno, 2012), the herbaceous layer is strongly
493 dependent on rainfall variations as it accesses water in the topsoil with a dense near-surface root system (Ward et al., 2013). It
494 is therefore much more sensitive to intra- and inter-annual climate variations (Luo et al., 2020). This is probably the reason
495 that the seasonal NEE variability was very low at all sites in 2017. We attribute this to extraordinary dryness in that year, as
496 dryness can lead to severe decreases in both GPP and R_{eco} in this type of ecosystem (Ma et al., 2007).

497



498

499 **Figure 6: Annual range of net ecosystem exchange (NEE) (i.e., maximum NEE minus minimum NEE) in gC m² y⁻¹ calculated using**
 500 **the seasonal reconstructed signal at the control site (CT), the nitrogen fertilized site (NT) and nitrogen + phosphorus fertilized site**
 501 **(NPT). The range at NPT (p-value = 0.049) significantly increased over 8 years, while not at NT (p-value = 0.116) and CT (p-value**
 502 **= 0.270).**

503

504 4.2 Key controls of seasonal NEE

505 Our results indicate that proxies for vegetation greenness (NDVI and GCC at grass layer derived from satellite and PhenoCam
 506 data, respectively) are the primary factors influencing the seasonal NEE signal in this ecosystem across treatments (Fig.3).
 507 However, depending on different seasons, other variables such as air temperatures, VPD, moisture-related variables, and soil
 508 temperatures can also be important.

509 Many studies identify NDVI, a proxy for vegetation greenness and photosynthesis, as a primary predictor of NEE (Del Grosso
 510 et al., 2018; Hermance et al., 2015; Morgan et al., 2016). NDVI, generally derived from satellite data, represents ecosystem
 511 greenness and its connection with ecosystem CO₂ fluxes has been intensively studied (Barnes et al., 2016; Hermance et al.,
 512 2015; Morgan et al., 2016; Running and Nemani, 1988). However, quantifying the importance of coexisting vegetation layers
 513 is more complex and less understood. Digital repeat cameras and vegetation greenness indices derived from them provide a
 514 powerful tool for analysing the greenness of different plant types (Migliavacca et al., 2011; Petach et al., 2014; Richardson et
 515 al., 2009; Yan et al., 2019) and their influence on ecosystem fluxes (Luo et al., 2018; Moore et al., 2017; Wingate et al., 2015).
 516 Our analysis confirms that grass layer dynamics are dominant in controlling seasonal ecosystem NEE at this site.

517 In situ measurements of vegetation greenness, however, are not available at all EC sites. We found that EF (i.e., evaporative
 518 fraction), representing the fraction of available energy transported by LE, is the third most important driver across treatments
 519 and methods on the synchronous scale. EF is strongly influenced by net radiation and water-related variables like soil moisture
 520 and VPD (Gentine et al., 2007; Tong et al., 2022). Since it depends on the portion of LE that is transpired by plants, it is also



521 impacted by LAI (Gentine et al., 2007). EF therefore serves as a bridge between meteorological and vegetation controls. We
522 suggest that at semi-arid sites where GCC measurements are not available, EF, calculated from measured LE and H, can serve
523 as important predictor of NEE.

524 In water-limited semi-arid ecosystems, NEE variations are typically dominated by soil-water related variables such as SWCn
525 and precipitation (Archibald et al., 2009; Baldocchi and Arias Ortiz, 2024; Huang et al., 2016b; Morgan et al., 2016). These
526 variables usually exert a greater influence than radiation and temperature (Del Grosso et al., 2018; Kannenberg et al., 2024).
527 Water availability promotes plant photosynthesis (Parton et al., 2012), but rain pulses can also enhance heterotrophic
528 respiration rates (Morgan et al., 2016). While we do not use precipitation data for the MI analysis, as it tends to be zero on
529 many days and cannot be used in MI (Gong et al., 2014), SWCn can capture topsoil moisture and indicate precipitation pulses.
530 Additionally, EF can serve as a proxy for these pulses. In our analysis we identify EF as one of the most important NEE drivers,
531 while other moisture-related variables (e.g., SWCn, VPD, Rh) are generally ranked lower in importance compared to air and
532 soil temperatures (Fig.3).

533 Air temperature can directly affect the speed of the enzyme responsible for carbon fixation and the rate of photosynthetic
534 electron transport (Leuning, 2002; Xu and Baldocchi, 2003). Additionally, temperature impacts the availability of
535 photosynthetic enzymes, membrane fluidity, and the expression of associated proteins (Yamori et al., 2014). However, our
536 results show that soil temperatures, both under oak trees and in open areas, play a significant role in explaining seasonal
537 ecosystem NEE variations (Fig.3), exceeding the importance of air temperatures. Soil respiration, one of the components in
538 R_{eco} , is highly sensitive to soil temperature (Conant et al., 2000), and elevated soil temperatures are associated with increased
539 soil respiration in semi-arid ecosystems (Richardson et al., 2012). These temperatures influence heterotrophic respiration,
540 which constitutes a substantial part of ecosystem NEE at our site (Casals et al., 2011). The high importance of soil temperatures
541 hints to R_{eco} dominating ecosystem processes and is especially relevant as the trend of increasing soil temperatures is stronger
542 than increasing air temperatures in the Mediterranean, particularly in grasslands with low soil moisture availability (Wang et
543 al., 2024).

544 Radiation parameters, in particular PAR, do not appear to play a crucial role on the seasonal scale. While other studies have
545 identified it as a major control of NEE in semi-arid ecosystems (Baldocchi and Arias Ortiz, 2024), we argue that PAR
546 predominantly influences the daily NEE signal (S1.2), but its importance diminishes on seasonal time scales.

547 Overall, we observe only marginal differences between the treatments when considering the 7-year period (2016-2022)
548 together. The added nutrients, particularly N, are primarily absorbed by the herbaceous layer (El-Madany et al., 2021) that
549 senesces annually. Consequently, some of the added nutrients may be lost from the system, diminishing the long-term effect
550 of the fertilization. By calculating MI_{sync} and MI_{max} for one year post-fertilization (March 2016-February 2017), we observe
551 greater differences between the three plots in MI values and lag times (S5). Additionally, the ecosystem is strongly water-
552 limited in the summer and energy-limited in the winter (Luo et al., 2018; Nair et al., 2019). These limitations can be more
553 pronounced than nutrient limitations in their respective seasons, overshadowing the effects of added nutrients when analysing



554 the entire dataset together. Therefore, we divided the dataset into five phenological seasons to gain deeper insights into how
555 added nutrients and altered stoichiometric balance affect seasonal NEE.

556 **4.3 Fertilization effects in different phenological seasons**

557 Looking into phenological seasons gives a deeper insight into how environmental variables influence seasonal NEE and how
558 N:P levels affect this relationship. We find that nutrient addition has an effect on NEE - control relationships when other
559 limitations are not too strong.

560 In the primary growing season, spring, NEE is dominated by GPP. The key drivers during this season across sites are NDVI
561 and GCC of both the herbaceous and tree layers (Table 2). Water is typically abundant promoting plant photosynthesis during
562 moderate temperatures in this time (Baldocchi and Arias Ortiz, 2024). These conditions are further supported by increased day
563 length and higher radiation levels (Luo et al., 2018). The rise in incoming radiation, extended daylight hours, and elevated
564 temperatures, coupled with the increased atmospheric evaporative demand (i.e., higher VPD), lead to a strong correlation
565 between precipitation and both GCC and GPP, as observed in various Mediterranean ecosystems (Diodato and Bellocchi, 2008;
566 Luo et al., 2018; Ma et al., 2007).

567 During the regreening of the herbaceous layer starting in autumn, NDVI shows the strongest interaction with NEE at the
568 fertilized plots - but not at the control plot. This aligns with previous studies showing that the green-up in this season happens
569 faster and the maximum GPP is higher at the fertilized plots, resulting from larger resource utilization at NT or improved
570 resource use efficiency at NPT (Luo et al., 2020). With the increase in soil moisture in early autumn, a greater quantity of
571 organic and inorganic nutrients becomes available to plants (Agehara and Warncke, 2005; Luo et al., 2020). N availability in
572 the soil is expected to be highest in this time (Morris et al., 2019), leading to higher net carbon uptake rates (El-Madany et al.,
573 2021). Leaves quickly expand and pigments rapidly increase during this green-up period (Croft et al., 2015). At CT, the green-
574 up happens later compared to the fertilized plots and NEE is dominated for a longer time by R_{eco} instead of photosynthetic
575 activity (Luo et al., 2020). Our results indicate that soil temperatures below oak trees are more important than those in open
576 areas during this season (Table 2). The carbon pools under oak trees are the largest, providing substantial material for
577 heterotrophic decomposition (Casals et al., 2009). During autumn, after a prolonged dry season where a significant amount of
578 litter and organic material has already been decomposed by microbes, litter remains available for further heterotrophic
579 decomposition mainly below the trees. This ongoing decomposition under oak trees contributes to R_{eco} , especially as the onset
580 of rains enhances microbial activity due to increased water availability (Borken and Matzner, 2009). Additionally, the topsoil
581 layer remains wet for longer after rain pulses under oak trees compared to open areas, as soil moisture is primarily influenced
582 by soil evaporation in this season as the soil is rather bare. Therefore, differences in soil respiration between open and shaded
583 pastures can also be attributed to variations soil moisture.

584 In winter, the ecosystem is energy-limited (Luo et al., 2018), therefore radiation components (i.e., PAR and SWDR) are
585 important predictors for NEE. Tree Albedo shows strong interactions with NEE at CT and NT, and NDVI shows strong
586 interactions with NEE at both fertilized plots. Plant growth is enhanced by added nutrients (Luo et al., 2020) and made available



587 by abundant water availability (Lee et al., 2010) in this season. Also, N+P addition can lead to an increased species diversity
588 due to alleviated nutrient limitation facilitating the co-existence of multiple species (Köbel et al., 2024). Additionally, EF
589 shares high mutual information with NEE variations. This is likely because respiration does not change significantly during
590 this period, and VPD is relatively low, leading to a strong coupling between NEE and LE. Additionally, in winter, the stomatal
591 control of the tree transpiration is not too strong, as soil water is abundant (Klein et al., 2013).

592 In the water-limited seasons, the nutrient effect is minimal as the grass layer is dormant and nutrients are not made available
593 due to a lack of water. During the drydown period, soil moisture (i.e., SWCn) decreases drastically due to increasing air
594 temperatures and scarce rainfall (Battista et al., 2018; Luo et al., 2018). This induces annual grasses to become senescent,
595 leading to a loss of chlorophyll content (Luo et al., 2018). The rate of this senescence can determine whether NEE becomes
596 positive or negative during this time. NDVI and grass layer GCC, the most important predictors of NEE in this season across
597 sites, can provide insights into the dry down rate. At NT grass layer GCC is less important, which we attribute to a more rapid
598 drydown, causing the grass layer to enter dormancy earlier than at other sites (Luo et al., 2020). This is because N addition
599 promotes faster water usage (Luo et al., 2020), accelerating the decrease in SWCn and thereby hampering photosynthesis. It
600 leads to a higher transpiration at NT compared to the other sites, potentially due to rhizosphere priming to increase P
601 mobilization through microbes, as adding only N to the system leads to a P deficiency (El-Madany et al., 2021). In addition,
602 N fertilization can alter species diversity and composition, likely selecting for species that senesce early (Wang and Tang,
603 2019). The higher interaction of soil temperatures with NEE in this season compared to the wetter seasons, show that R_{eco}
604 starts dominating NEE, as R_{eco} is strongly connected to soil temperatures (Metz et al., 2023). VPD is a stronger control of NEE
605 at NT compared to the other two plots. Transpiration is highest at NT, as plants transpire more to obtain limited P from the
606 soil (El-Madany et al., 2021; Pang et al., 2018; Rose et al., 2018). It is therefore more sensitive to changes in VPD.

607 In summer, the driest period at the ecosystem, R_{eco} dominates NEE and thus we find a strong interaction between NEE and
608 soil temperature and soil heat flux (i.e., SHF_Sun and SHF_Sh). Besides, PAR is important for predicting seasonal NEE,
609 showing the strongest interaction at CT. The importance of PAR is lower at NT and lowest at NPT. N+P addition increases
610 the light use efficiency most because P has a positive effect on photochemical quenching in leaves and on active fluorescence
611 measurements (Martini et al., 2019; Singh and Reddy, 2014), leading to less dependency of NEE to radiation parameters at
612 that site. At CT and NT, tree layer GCC is important as the grass layer becomes senescent in the summer and is dormant in
613 terms of ecosystem carbon flux. Since the greenness of the oak trees is constant throughout the year, GPP is mainly determined
614 by the tree layer in the summer months (Luo et al., 2018). However, gcc_{gr} shows a higher interaction with NEE than gcc_{tr}
615 at NPT. Even though most of the grass layer is mostly dead in this season, there are some perennial species (e.g. *cynodon*
616 *dactylon*) remaining green for longer in summer and can regreen after any rain events (personal communication with local
617 collaborators). Therefore, N+P addition very likely leads to a consequential change in species composition (Köbel et al., 2024)
618 with an increase in these perennial species or results in an increase in their productivity. So far it has been found that N+P
619 addition can lead to an increasing number of forbs (Köbel et al., 2024), which tend to senesce later than other herbaceous



620 species at the site (Luo et al., 2020). Nevertheless, the occurrence of summer-green species following nutrient addition will
621 have to be investigated further.

622 The analysis of driver importance in different phenological seasons provides significant insights into ecosystem processes.
623 However, some variables must be interpreted with caution. The soil properties at this site are highly heterogeneous, which
624 affects the representativity of variables like soil temperature, soil water content and soil heat flux in the EC flux footprint (Luo
625 et al., 2018; Paulus et al., 2022). This is particularly relevant given the substantial differences between below-canopy and
626 open-air soil conditions. To address this, we have separated the measurements into areas under the oak tree canopy and sunlit
627 areas (T_{soilShd} and SHF_{Shd} , and T_{soilSun} and SHF_{Sun}). Despite this effort, the local soil heterogeneity is more complex,
628 influenced by varying proportions of sand, clay, and soil organic carbon (Casals et al., 2011; Weiner et al., 2018). Therefore,
629 it is important to consider that these measures may not fully capture the sensitivity differences in the ecosystem.

630 **4.4 Future implications**

631 In winter, the ecosystem has abundant water availability, and energy becomes the primary limiting factor after nutrients were
632 added. With N only addition, we observe that NEE becomes significantly more sensitive to changes in the radiation
633 components, PAR and SWDR (Fig.5). However, the addition of N+P results in a significant increase in sensitivity to changes
634 in soil water content rather than radiation components. N+P addition enhances water use efficiency in the ecosystem (El-
635 Madany et al., 2021; Martini et al., 2019), and consequently, water can be used more efficiently for photosynthesis with
636 similarly low radiation levels and increased water availability could lead to a higher GPP. N fertilization primarily affects the
637 herbaceous layer (El-Madany et al., 2021), and our results agree with this, showing a significantly increased sensitivity of NEE
638 to grass layer greenness in winter at NT and an even steeper increase at NPT (Fig.5). At N+P plot there are more nutrients
639 available at a higher N:P stoichiometric balance.

640 In spring, the sensitivity to tree layer greenness decreases with N fertilization. An experimental study by Biro et al. (2024)
641 supports these findings, demonstrating that N addition results in decreased tree growth due to competition with grass, which
642 also intensively forages for P. The study suggests that grasses likely prevail in below-ground competition, primarily due to
643 their substantial root biomass allocation and investment in nutrient-acquiring enzymes, such as phosphatase. These adaptations
644 enable grasses to efficiently sequester both N and P from the soil, thereby outcompeting trees for these essential nutrients (Biro
645 et al., 2024; Rolo and Moreno, 2012). With the addition of N+P, we observe that the NEE sensitivity to PAR increases
646 significantly in spring (Fig.5). Water and nutrients are abundant in this season at NPT, making the availability of energy more
647 crucial.

648 In the water-limited seasons, ecosystem processes behave quite differently and we observe less effect of nutrient addition.
649 With N+P addition, there is no significant trend in NEE sensitivity to its drivers, except for a significantly increased sensitivity
650 to grass layer greenness in summer. This agrees with our previous findings that in summer gcc_{gr} is amongst the most
651 important drivers at NPT (Table 2). This reflects changes in the species decomposition with N+P fertilization, enhancing



652 especially the growth and diversity of forbs and perennial species. We argue that long-term N+P addition could even lead to
653 an increased productivity, leading to an increasing importance of grass layer greenness for ecosystem NEE.

654 The significant increase of the yearly NEE range at NPT over time (Fig.6) is very likely caused by the increased NEE sensitivity
655 to drivers in spring and summer, as the minimum NEE (usually occurring in spring) becoming more negative and maximum
656 NEE (usually occurring in summer) becoming more positive. Consequently, the increased NEE sensitivity to changes in PAR
657 in spring and increased sensitivity to gcc_gr in summer might enhance the size of this annual range.

658 In the drydown phase we observe that with N addition, the sensitivity of ecosystem NEE to changes in relative humidity (i.e.,
659 Rh02 and Rh15) and SHF_Sun decreases significantly. This indicates that the ecosystem might become more resistant against
660 variations in these variables in the future.

661 In autumn both fertilized sites become less sensitive to changes in atmospheric variables such as the radiation components
662 PAR and SWDR, air temperatures and VPD, compared to the control plot. This indicates that water availability is
663 predominantly important for NEE with added nutrients, and the sensitivity to the other variables decreases. It is possible that
664 either the vegetations or the microbes become less restricted by these variables.

665 We conclude that with more N-input from human activities entering terrestrial ecosystems (Penuelas et al., 2013), savannas
666 may become less sensitive to environmental factors like humidity, radiation, and temperature during the transitional seasons
667 (i.e., drydown and regreening). These seasons determine the start and end of an active grass layer and therefore dominate the
668 annual carbon balance of the ecosystem. In addition, we expect the NEE variability to increase even more in the future with
669 more N deposition and a changing climate. To note, the results of this study cannot explain on how the long-term nutrient
670 addition affects the ecosystems resistance to extreme events.

671

672 5 Conclusion

673 We analysed a long-term (2016-2022/23) dataset of flux, biometeorological, satellite and PhenoCam data from the semi-arid
674 experimental site, Majadas de Tiétar, to evaluate the importance of different drivers for NEE across three different nutrient
675 balances. To detect the most important drivers, we used only daytime daily values of observed data to extract the seasonal
676 signal of all variables using the Singular Spectrum Analysis.

677 With both Pearson correlation and mutual information analysis we show that the grass layer drives seasonal variations in NEE
678 across all treatments, and that both N and N+P addition increases the seasonal NEE variability. We find that soil temperatures
679 are more important in explaining NEE variations than previously expected. When looking into the entire 7-year data together,
680 the water and energy limitation cycles overshadows the nutrient addition effect. Dividing the dataset into phenological seasons
681 reveals how environmental variables and nutrient manipulation influenced NEE on a seasonal scale. Altered nutrient levels
682 affect NEE-control relationships when water and energy limitations are not too strong, particularly during the primary growing
683 season in spring, where NDVI and grass layer GCC are key drivers. In autumn, NDVI shows the strongest interaction with



684 NEE at fertilized plots, indicating faster green-up and higher GPP due to enhanced nutrient availability. During drier seasons,
685 nutrient effects are less pronounced as the grass layer becomes dormant.
686 N and N+P additions significantly alters the sensitivity of NEE to environmental controls over time. In winter, N addition
687 increases NEE sensitivity to radiation, while N+P addition increases its sensitivity to changes in soil water content. In spring,
688 N+P addition increases sensitivity to PAR. The herbaceous layer primarily benefits from nutrient additions, leading to
689 increased sensitivity of NEE to grass layer greenness and decreased sensitivity to tree layer greenness. During water-limited
690 seasons, nutrient effects were minimal, except for increased importance of grass layer GCC in summer at NPT, indicating an
691 increase in abundance and/or productivity with N+P treatment due to changed species composition and higher biodiversity.
692 We conclude that with increasing anthropogenic N deposition the carbon dynamics of savannas might become even more
693 variable in the future, but more resistant to variations in some atmospheric variables in the transitional seasons, which
694 determine the annual carbon balance of the ecosystem. However, their responses to extreme events in the future remains to be
695 explored.

696 **Data Availability**

697 Ecosystem level data is available on the European Fluxes Database (<https://www.europe-fluxdata.eu/>) and PhenoCam
698 (<https://phenocam.nau.edu/webcam/>). The FluxnetEO dataset can be found on the ICOS Carbon Portal.

699 **Author Contributions**

700 LN: Conceptualization, Data curation, Methodology, Formal analysis, Writing – original draft preparation. TE: Data curation,
701 Writing - review & editing. JN: Writing – review & editing. AC: Data curation, Writing – review & editing. GM: Data curation,
702 Writing – review & editing. RN: Software, Writing – review & editing. YL: Software, Writing – review & editing. AH:
703 Supervision, Writing – review & editing. VR: Data curation. Writing - review & editing. MR: Resources, Funding acquisition,
704 Writing – review & editing. SL: Conceptualization, Methodology, Supervision, Writing – review & editing.

705 **Declaration of Competing Interest**

706 The authors declare that they have no known competing financial interests or personal relationships that could have appeared
707 to influence the work reported in this paper.



708 Acknowledgements

709 We thank Mirco Migliavacca (European Commission, Joint Research Centre, Ispra, Varese, Italy) for sharing advice and
710 expertise, the Freiland Group at Max-Planck Institute for Biogeochemistry in Jena for maintaining and calibrating sites and
711 sensors, as well as Ramón López for daily data collection and site maintenance.

712 The nutrient manipulation experiment was funded by the Alexander von Humboldt Foundation Max Planck Research Prize to
713 Markus Reichstein (i.e., MANIP project). Laura Nadolski received financial support from the International Max Planck
714 Research School for Biogeochemical Cycles (IMPRS-gBGC).

715

716 References

717 Agehara, S. and Warncke, D. D.: Soil Moisture and Temperature Effects on Nitrogen Release from Organic Nitrogen Sources,
718 Soil Science Soc of Amer J, 69, 1844–1855, <https://doi.org/10.2136/sssaj2004.0361>, 2005.

719 Ahlström, A., Raupach, M. R., Schurgers, G., Smith, B., Arneth, A., Jung, M., Reichstein, M., Canadell, J. G., Friedlingstein,
720 P., Jain, A. K., Kato, E., Poulter, B., Sitch, S., Stocker, B. D., Viovy, N., Wang, Y. P., Wiltshire, A., Zaehle, S., and Zeng, N.:
721 The dominant role of semi-arid ecosystems in the trend and variability of the land CO₂ sink, Science, 348, 895–899,
722 <https://doi.org/10.1126/science.aaa1668>, 2015.

723 Allen, M. R. and Smith, L. A.: Monte Carlo SSA: Detecting irregular oscillations in the Presence of Colored Noise, J. Climate,
724 9, 3373–3404, [https://doi.org/10.1175/1520-0442\(1996\)009<3373:MCSPIO>2.0.CO;2](https://doi.org/10.1175/1520-0442(1996)009<3373:MCSPIO>2.0.CO;2), 1996.

725 Arca, V., Power, S. A., Delgado-Baquerizo, M., Pendall, E., and Ochoa-Hueso, R.: Seasonal effects of altered precipitation
726 regimes on ecosystem-level CO₂ fluxes and their drivers in a grassland from Eastern Australia, Plant Soil, 460, 435–451,
727 <https://doi.org/10.1007/s11104-020-04811-x>, 2021.

728 Archibald, S. A., Kirton, A., van der Merwe, M. R., Scholes, R. J., Williams, C. A., and Hanan, N.: Drivers of inter-annual
729 variability in Net Ecosystem Exchange in a semi-arid savanna ecosystem, South Africa, Biogeosciences, 6, 251–266,
730 <https://doi.org/DOI.10.5194/bg-6-251-2009>, 2009.

731 Bachofen, C., Tumber-Dávila, S. J., Mackay, D. S., McDowell, N. G., Carminati, A., Klein, T., Stocker, B. D., Mencuccini,
732 M., and Grossiord, C.: Tree water uptake patterns across the globe, New Phytologist, 242, 1891–1910,
733 <https://doi.org/10.1111/nph.19762>, 2024.

734 Baldocchi, Ma, S. Y., and Verfaillie, J.: On the inter- and intra-annual variability of ecosystem evapotranspiration and water
735 use efficiency of an oak savanna and annual grassland subjected to booms and busts in rainfall, Global Change Biol, 27, 359–
736 375, <https://doi.org/10.1111/gcb.15414>, 2021.

737 Baldocchi, D. D. and Arias Ortiz, A.: Alternating Conditional Expectations: Introducing a Non-Parametric Statistical Method
738 to Interpret Long-Term Greenhouse Gas Flux Measurements Over Semi-Arid and Wetland Ecosystems, JGR Biogeosciences,
739 129, e2023JG007818, <https://doi.org/10.1029/2023JG007818>, 2024.

740 Baldocchi, D. D., Xu, L., and Kiang, N.: How plant functional-type, weather, seasonal drought, and soil physical properties
741 alter water and energy fluxes of an oak–grass savanna and an annual grassland, Agricultural and Forest Meteorology, 123, 13–
742 39, <https://doi.org/10.1016/j.agrformet.2003.11.006>, 2004.



- 743 Barnes, M. L., Moran, M. S., Scott, R. L., Kolb, T. E., Ponce-Campos, G. E., Moore, D. J. P., Ross, M. A., Mitra, B., and
744 Dore, S.: Vegetation productivity responds to sub-annual climate conditions across semiarid biomes, *Ecosphere*, 7, e01339,
745 <https://doi.org/10.1002/ecs2.1339>, 2016.
- 746 Battista, P., Chiesi, M., Fibbi, L., Gardin, L., Rapi, B., Romanelli, S., Romani, M., Sabatini, F., Salerni, E., Perini, C., and
747 Maselli, F.: Simulation of Soil Water Content in Mediterranean Ecosystems by Biogeochemical and Remote Sensing Models,
748 *Water*, 10, 665, <https://doi.org/10.3390/w10050665>, 2018.
- 749 Bernacchi, C. J., Singsaas, E. L., Pimentel, C., Portis Jr, A. R., and Long, S. P.: Improved temperature response functions for
750 models of Rubisco-limited photosynthesis, *Plant Cell & Environment*, 24, 253–259, <https://doi.org/10.1111/j.1365-3040.2001.00668.x>, 2001.
- 752 Biriukova, K., Pacheco-Labrador, J., Migliavacca, M., Mahecha, M. D., Gonzalez-Cascon, R., Martin, M. P., and Rossini, M.:
753 Performance of Singular Spectrum Analysis in Separating Seasonal and Fast Physiological Dynamics of Solar-Induced
754 Chlorophyll Fluorescence and PRI Optical Signals, *J Geophys Res-Biogeophys*, 126, <https://doi.org/ARTN e2020JG006158>
755 10.1029/2020JG006158, 2021.
- 756 Biro, A., Wong, M. Y., Zhou, Y., Batterman, S. A., and Staver, A. C.: Nitrogen and phosphorus availability alters tree-grass
757 competition intensity in savannas, *Journal of Ecology*, 112, 1026–1038, <https://doi.org/10.1111/1365-2745.14284>, 2024.
- 758 Bogdanovich, E., Perez-Priego, O., El-Madany, T. S., Guderle, M., Pacheco-Labrador, J., Levick, S. R., Moreno, G., Carrara,
759 A., Martin, M. P., and Migliavacca, M.: Using terrestrial laser scanning for characterizing tree structural parameters and their
760 changes under different management in a Mediterranean open woodland, *Forest Ecol Manag*, 486, <https://doi.org/ARTN 118945>
761 10.1016/j.foreco.2021.118945, 2021.
- 762 Borken, W. and Matzner, E.: Reappraisal of drying and wetting effects on C and N mineralization and fluxes in soils, *Global
763 Change Biol*, 15, 808–824, <https://doi.org/10.1111/j.1365-2486.2008.01681.x>, 2009.
- 764 Buttlar, J. von: An extended approach for spatiotemporal gapfilling: dealing with large and systematic gaps in geoscientific
765 datasets, *Nonlinear Processes in Geophysics*, 21, 203–215, <https://doi.org/doi:10.5194/npg-21-203-2014>, 2014.
- 766 Casals, P., Gimeno, C., Carrara, A., Lopez-Sangil, L., and Sanz, M. J.: Soil CO₂ efflux and extractable organic carbon fractions
767 under simulated precipitation events in a Mediterranean Dehesa, *Soil Biol Biochem*, 41, 1915–1922,
768 <https://doi.org/10.1016/j.soilbio.2009.06.015>, 2009.
- 769 Casals, P., Lopez-Sangil, L., Carrara, A., Gimeno, C., and Nogues, S.: Autotrophic and heterotrophic contributions to short-
770 term soil CO₂ efflux following simulated summer precipitation pulses in a Mediterranean dehesa, *Global Biogeochem Cy*, 25,
771 <https://doi.org/Artn Gb3012> 10.1029/2010gb003973, 2011.
- 772 Chamberlain, S. D., Anthony, T. L., Silver, W. L., Eichelmann, E., Hemes, K. S., Oikawa, P. Y., Sturtevant, C., Szutu, D. J.,
773 Verfaillie, J. G., and Baldocchi, D. D.: Soil properties and sediment accretion modulate methane fluxes from restored wetlands,
774 *Glob Change Biol*, 24, 4107–4121, <https://doi.org/10.1111/gcb.14124>, 2018.
- 775 Chamberlain, S. D., Hemes, K. S., Eichelmann, E., Szutu, D. J., Verfaillie, J. G., and Baldocchi, D. D.: Effect of Drought-
776 Induced Salinization on Wetland Methane Emissions, Gross Ecosystem Productivity, and Their Interactions, *Ecosystems*, 23,
777 675–688, <https://doi.org/10.1007/s10021-019-00430-5>, 2020.
- 778 Conant, R. T., Klopatek, J. M., and Klopatek, C. C.: Environmental Factors Controlling Soil Respiration in Three Semiarid
779 Ecosystems, *Soil Science Soc of Amer J*, 64, 383–390, <https://doi.org/10.2136/sssaj2000.641383x>, 2000.



- 780 Croft, H., Chen, J. M., Froelich, N. J., Chen, B., and Staebler, R. M.: Seasonal controls of canopy chlorophyll content on forest
781 carbon uptake: Implications for GPP modeling, *JGR Biogeosciences*, 120, 1576–1586, <https://doi.org/10.1002/2015JG002980>,
782 2015.
- 783 Del Grosso, S. J., Parton, W. J., Derner, J. D., Chen, M. S., and Tucker, C. J.: Simple models to predict grassland ecosystem
784 C exchange and actual evapotranspiration using NDVI and environmental variables, *Agricultural and Forest Meteorology*,
785 249, 1–10, <https://doi.org/10.1016/j.agrformet.2017.11.007>, 2018.
- 786 Den Herder, M., Moreno, G., Mosquera-Losada, R. M., Palma, J. H. N., Sidiropoulou, A., Santiago Freijanes, J. J., Crous-
787 Duran, J., Paulo, J. A., Tomé, M., Pantera, A., Papanastasis, V. P., Mantzanas, K., Pachana, P., Papadopoulos, A., Plieninger,
788 T., and Burgess, P. J.: Current extent and stratification of agroforestry in the European Union, *Agriculture, Ecosystems &*
789 *Environment*, 241, 121–132, <https://doi.org/10.1016/j.agee.2017.03.005>, 2017.
- 790 Diodato, N. and Bellocchi, G.: Modelling vegetation greenness responses to climate variability in a Mediterranean terrestrial
791 ecosystem, *Environ Monit Assess*, 143, 147–159, <https://doi.org/10.1007/s10661-007-9964-z>, 2008.
- 792 Dubbert, M., Piayda, A., Cuntz, M., Correia, A. C., Silva, F. C. E., Pereira, J. S., and Werner, C.: Stable oxygen isotope and
793 flux partitioning demonstrates understory of an oak savanna contributes up to half of ecosystem carbon and water exchange,
794 *Front Plant Sci*, 5, <https://doi.org/ARTN 530 10.3389/fpls.2014.00530>, 2014.
- 795 El-Madany, T. S., Reichstein, M., Perez-Priego, O., Carrara, A., Moreno, G., Martin, M. P., Pacheco-Labrador, J., Wohlfahrt,
796 G., Nieto, H., Weber, U., Kolle, O., Luo, Y. P., Carvalhais, N., and Migliavacca, M.: Drivers of spatio-temporal variability of
797 carbon dioxide and energy fluxes in a Mediterranean savanna ecosystem, *Agricultural and Forest Meteorology*, 262, 258–278,
798 <https://doi.org/10.1016/j.agrformet.2018.07.010>, 2018.
- 799 El-Madany, T. S., Carrara, A., Martin, M. P., Moreno, G., Kolle, O., Pacheco-Labrador, J., Weber, U., Wutzler, T., Reichstein,
800 M., and Migliavacca, M.: Drought and heatwave impacts on semi-arid ecosystems' carbon fluxes along a precipitation
801 gradient, *Philos T R Soc B*, 375, <https://doi.org/ARTN 20190519 10.1098/rstb.2019.0519>, 2020.
- 802 El-Madany, T. S., Reichstein, M., Carrara, A., Martin, M. P., Moreno, G., Gonzalez-Cascon, R., Penuelas, J., Ellsworth, D.
803 S., Burchard-Levine, V., Hammer, T. W., Knauer, J., Kolle, O., Luo, Y. P., Pacheco-Labrador, J., Nelson, J. A., Perez-Priego,
804 O., Rolo, V., Wutzler, T., and Migliavacca, M.: How Nitrogen and Phosphorus Availability Change Water Use Efficiency in
805 a Mediterranean Savanna Ecosystem, *J Geophys Res-Biogeophys*, 126, [https://doi.org/ARTN e2020JG006005](https://doi.org/ARTN e2020JG006005 10.1029/2020JG006005)
806 10.1029/2020JG006005, 2021.
- 807 Fawcett, D., Cunliffe, A. M., Sitch, S., O'Sullivan, M., Anderson, K., Brazier, R. E., Hill, T. C., Anthoni, P., Arneth, A., Arora,
808 V. K., Briggs, P. R., Goll, D. S., Jain, A. K., Li, X., Lombardozzi, D., Nabel, J. E. M. S., Poulter, B., Séférian, R., Tian, H.,
809 Viovy, N., Wigneron, J.-P., Wiltshire, A., and Zaehle, S.: Assessing Model Predictions of Carbon Dynamics in Global
810 Drylands, *Front. Environ. Sci.*, 10, 790200, <https://doi.org/10.3389/fenvs.2022.790200>, 2022.
- 811 Fleischer, K., Rebel, K. T., Van Der Molen, M. K., Erisman, J. W., Wassen, M. J., Van Loon, E. E., Montagnani, L., Gough,
812 C. M., Herbst, M., Janssens, I. A., Gianelle, D., and Dolman, A. J.: The contribution of nitrogen deposition to the
813 photosynthetic capacity of forests, *Global Biogeochemical Cycles*, 27, 187–199, <https://doi.org/10.1002/gbc.20026>, 2013.
- 814 Fraser, A. M. and Swinney, H. L.: Independent coordinates for strange attractors from mutual information, *Phys. Rev. A*, 33,
815 1134–1140, <https://doi.org/10.1103/PhysRevA.33.1134>, 1986.
- 816 Fratini, G. and Mauder, M.: Towards a consistent eddy-covariance processing: an intercomparison of EddyPro and TK3,
817 *Atmos. Meas. Tech.*, 7, 2273–2281, <https://doi.org/10.5194/amt-7-2273-2014>, 2014.



- 818 Friedlingstein, P., O’Sullivan, M., Jones, M. W., Andrew, R. M., Gregor, L., Hauck, J., Le Quere, C., Luijkx, I. T., Olsen, A.,
819 Peters, G. P., Peters, W., Pongratz, J., Schwingshackl, C., Sitch, S., Canadell, J. G., Ciais, P., Jackson, R. B., Alin, S. R.,
820 Alkama, R., Arneeth, A., Arora, V. K., Bates, N. R., Becker, M., Bellouin, N., Bittig, H. C., Bopp, L., Chevallier, F., Chini, L.
821 P., Cronin, M., Evans, W., Falk, S., Feely, R. A., Gasser, T., Gehlen, M., Gkritzalis, T., Gloege, L., Grassi, G., Gruber, N.,
822 Gurses, O., Harris, I., Hefner, M., Houghton, R. A., Hurtt, G. C., Iida, Y., Ilyina, T., Jain, A. K., Jersild, A., Kadono, K., Kato,
823 E., Kennedy, D., Goldewijk, K. K., Knauer, J., Korsbakken, J. I., Landschutzer, P., Lefevre, N., Lindsay, K., Liu, J. J., Liu, Z.,
824 Marland, G., Mayot, N., McGrath, M. J., Metz, N., Monacchi, N. M., Munro, D. R., Nakaoka, S. I., Niwa, Y., O’Brien, K.,
825 Ono, T., Palmer, P. I., Pan, N. Q., Pierrot, D., Pockock, K., Poulter, B., Resplandy, L., Robertson, E., Rodenbeck, C., Rodriguez,
826 C., Rosan, T. M., Schwinger, J., Seferian, R., Shutler, J. D., Skjelvan, I., Steinhoff, T., Sun, Q., Sutton, A. J., Sweeney, C.,
827 Takao, S., Tanhua, T., Tans, P. P., Tian, X. J., Tian, H. Q., Tilbrook, B., Tsujino, H., Tubiello, F., van der Werf, G. R., Walker,
828 A. P., Wanninkhof, R., Whitehead, C., Wranne, A. W., et al.: Global Carbon Budget 2022, *Earth Syst Sci Data*, 14, 4811–
829 4900, <https://doi.org/10.5194/essd-14-4811-2022>, 2022.
- 830 Gentine, P., Entekhabi, D., Chehbouni, A., Boulet, G., and Duchemin, B.: Analysis of evaporative fraction diurnal behaviour,
831 *Agricultural and Forest Meteorology*, 143, 13–29, <https://doi.org/10.1016/j.agrformet.2006.11.002>, 2007.
- 832 Giorgi, F. and Lionello, P.: Climate change projections for the Mediterranean region, *Global and Planetary Change*, 63, 90–
833 104, <https://doi.org/10.1016/j.gloplacha.2007.09.005>, 2008.
- 834 Golyandina, N. and Korobeynikov, A.: Basic Singular Spectrum Analysis and forecasting with R, *Comput Stat Data An*, 71,
835 934–954, <https://doi.org/10.1016/j.csda.2013.04.009>, 2014.
- 836 Golyandina, N. and Zhigljavsky, A.: *Singular Spectrum Analysis for Time Series*, Springer Berlin Heidelberg, Berlin,
837 Heidelberg, <https://doi.org/10.1007/978-3-642-34913-3>, 2013.
- 838 Golyandina, N., Nekrutin, V., and Zhigljavsky, A.: *Analysis of Time Series Structure. SSA and Related Techniques*, Chapman
839 & Hall/CRC, Boca Raton, London, New York, Washington D.C., 2001.
- 840 Golyandina, N., Korobeynikov, A., and Zhigljavsky, A.: *Singular Spectrum Analysis*, Springer, Berlin, Germany, 2018.
- 841 Gong, W., Yang, D., Gupta, H. V., and Nearing, G.: Estimating information entropy for hydrological data: One-dimensional
842 case, *Water Resources Research*, 50, 5003–5018, <https://doi.org/10.1002/2014WR015874>, 2014.
- 843 Haverd, V., Ahlstrom, A., Smith, B., and Canadell, J. G.: Carbon cycle responses of semi-arid ecosystems to positive
844 asymmetry in rainfall, *Global Change Biol*, 23, 793–800, <https://doi.org/10.1111/gcb.13412>, 2017.
- 845 Hermance, J. F., Augustine, D. J., and Derner, J. D.: Quantifying characteristic growth dynamics in a semi-arid grassland
846 ecosystem by predicting short-term NDVI phenology from daily rainfall: a simple four parameter coupled-reservoir model,
847 *International Journal of Remote Sensing*, 36, 5637–5663, <https://doi.org/10.1080/01431161.2015.1103916>, 2015.
- 848 Huang, Liu, B., Davis, M., Sardans, J., Penuelas, J., and Billings, S.: Long-term nitrogen deposition linked to reduced water
849 use efficiency in forests with low phosphorus availability, *New Phytol*, 210, 431–442, <https://doi.org/10.1111/nph.13785>,
850 2016a.
- 851 Huang, L., He, B., Chen, A., Wang, H., Liu, J., Lü, A., and Chen, Z.: Drought dominates the interannual variability in global
852 terrestrial net primary production by controlling semi-arid ecosystems, *Sci Rep*, 6, 24639, <https://doi.org/10.1038/srep24639>,
853 2016b.



- 854 Huxman, T. E., Snyder, K. A., Tissue, D., Leffler, A. J., Ogle, K., Pockman, W. T., Sandquist, D. R., Potts, D. L., and
855 Schwinning, S.: Precipitation pulses and carbon fluxes in semiarid and arid ecosystems, *Oecologia*, 141, 254–268,
856 <https://doi.org/10.1007/s00442-004-1682-4>, 2004.
- 857 Jung, M., Schwalm, C., Migliavacca, M., Walther, S., Camps-Valls, G., Koirala, S., Anthoni, P., Besnard, S., Bodesheim, P.,
858 Carvalhais, N., Chevallier, F., Gans, F., Goll, D. S., Haverd, V., Köhler, P., Ichii, K., Jain, A. K., Liu, J., Lombardozzi, D.,
859 Nabel, J. E. M. S., Nelson, J. A., O’Sullivan, M., Pallandt, M., Papale, D., Peters, W., Pongratz, J., Rödenbeck, C., Sitch, S.,
860 Tramontana, G., Walker, A., Weber, U., and Reichstein, M.: Scaling carbon fluxes from eddy covariance sites to globe:
861 synthesis and evaluation of the FLUXCOM approach, *Biogeosciences*, 17, 1343–1365, [https://doi.org/10.5194/bg-17-1343-](https://doi.org/10.5194/bg-17-1343-2020)
862 2020, 2020.
- 863 Kannenberg, S. A., Anderegg, W. R. L., Barnes, M. L., Dannenberg, M. P., and Knapp, A. K.: Dominant role of soil moisture
864 in mediating carbon and water fluxes in dryland ecosystems, *Nat. Geosci.*, 17, 38–43, [https://doi.org/10.1038/s41561-023-](https://doi.org/10.1038/s41561-023-01351-8)
865 01351-8, 2024.
- 866 Klein, T., Shpringer, I., Fikler, B., Elbaz, G., Cohen, S., and Yakir, D.: Relationships between stomatal regulation, water-use,
867 and water-use efficiency of two coexisting key Mediterranean tree species, *Forest Ecology and Management*, 302, 34–42,
868 <https://doi.org/10.1016/j.foreco.2013.03.044>, 2013.
- 869 Knox, S. H., Windham-Myers, L., Anderson, F., Sturtevant, C., and Bergamaschi, B.: Direct and Indirect Effects of Tides on
870 Ecosystem-Scale CO₂ Exchange in a Brackish Tidal Marsh in Northern California, *J Geophys Res-Biogeophys*, 123, 787–806,
871 <https://doi.org/10.1002/2017jg004048>, 2018.
- 872 Knox, S. H., Bansal, S., McNicol, G., Schafer, K., Sturtevant, C., Ueyama, M., Valach, A. C., Baldocchi, D., Delwiche, K.,
873 Desai, A. R., Euskirchen, E., Liu, J. X., Lohila, A., Malhotra, A., Melling, L., Riley, W., Runkle, B. R. K., Turner, J., Vargas,
874 R., Zhu, Q., Alto, T., Fluet-Chouinard, E., Goeckede, M., Melton, J. R., Sonnentag, O., Vesala, T., Ward, E., Zhang, Z., Feron,
875 S., Ouyang, Z. T., Alekseychik, P., Aurela, M., Bohrer, G., Campbell, D. I., Chen, J. Q., Chu, H. S., Dalmagro, H. J., Goodrich,
876 J. P., Gottschalk, P., Hirano, T., Iwata, H., Jurasinski, G., Kang, M., Koebsch, F., Mammarella, I., Nilsson, M. B., Ono, K.,
877 Peichl, M., Peltola, O., Ryu, Y., Sachs, T., Sakabe, A., Sparks, J. P., Tuittila, E. S., Vourlitis, G. L., Wong, G. X., Windham-
878 Myers, L., Poulter, B., and Jackson, R. B.: Identifying dominant environmental predictors of freshwater wetland methane
879 fluxes across diurnal to seasonal time scales, *Global Change Biol*, 27, 3582–3604, <https://doi.org/10.1111/gcb.15661>, 2021.
- 880 Köbel, M., Chozas, S., Moreno, G., Migliavacca, M., Branquinho, C., and Nunes, A.: Grasses don’t always win: Short-term
881 effects of fertilization on taxonomic and functional diversity of a Mediterranean annual grassland, *Agriculture, Ecosystems &*
882 *Environment*, 373, 109125, <https://doi.org/10.1016/j.agee.2024.109125>, 2024.
- 883 Kondrashov, D. and Ghil, M.: Spatio-temporal filling of missing points in geophysical data sets, *Nonlinear Processes in*
884 *Geophysics*, 13, 151–159, <https://doi.org/DOI.10.5194/npg-13-151-2006>, 2006.
- 885 Lee, M., Manning, P., Rist, J., Power, S. A., and Marsh, C.: A global comparison of grassland biomass responses to CO₂ and
886 nitrogen enrichment, *Phil. Trans. R. Soc. B*, 365, 2047–2056, <https://doi.org/10.1098/rstb.2010.0028>, 2010.
- 887 Leuning, R.: Temperature dependence of two parameters in a photosynthesis model, *Plant Cell & Environment*, 25, 1205–
888 1210, <https://doi.org/10.1046/j.1365-3040.2002.00898.x>, 2002.
- 889 Linscheid, N., Estupinan-Suarez, L. M., Brenning, A., Caryalhais, N., Cremer, F., Gans, F., Rammig, A., Reichstein, M.,
890 Sierra, C. A., and Mahecha, M. D.: Towards a global understanding of vegetation-climate dynamics at multiple timescales,
891 *Biogeosciences*, 17, 945–962, <https://doi.org/10.5194/bg-17-945-2020>, 2020.



- 892 Liu, J. G., Valach, A., Baldocchi, D., and Lai, D. Y. F.: Biophysical Controls of Ecosystem-Scale Methane Fluxes From a
893 Subtropical Estuarine Mangrove: Multiscale, Nonlinearity, Asynchrony and Causality, *Global Biogeochem Cy*, 36,
894 <https://doi.org/ARTN e2021GB007179> 10.1029/2021GB007179, 2022.
- 895 Luo, El-Madany, T. S., Filippa, G., Ma, X. L., Ahrens, B., Carrara, A., Gonzalez-Cascon, R., Cremonese, E., Galvagno, M.,
896 Hammer, T. W., Pacheco-Labrador, J., Martin, M. P., Moreno, G., Perez-Priego, O., Reichstein, M., Richardson, A. D.,
897 Romermann, C., and Migliavacca, M.: Using Near-Infrared-Enabled Digital Repeat Photography to Track Structural and
898 Physiological Phenology in Mediterranean Tree-Grass Ecosystems, *Remote Sens-Basel*, 10, <https://doi.org/ARTN 1293>
899 10.3390/rs10081293, 2018.
- 900 Luo, El-Madany, T., Ma, X. L., Nair, R., Jung, M., Weber, U., Filippa, G., Bucher, S. F., Moreno, G., Cremonese, E., Carrara,
901 A., Gonzalez-Cascon, R., Escudero, Y. C., Galvagno, M., Pacheco-Labrador, J., Martin, M. P., Perez-Priego, O., Reichstein,
902 M., Richardson, A. D., Menzel, A., Romermann, C., and Migliavacca, M.: Nutrients and water availability constrain the
903 seasonality of vegetation activity in a Mediterranean ecosystem, *Global Change Biol*, 26, 4379–4400,
904 <https://doi.org/10.1111/gcb.15138>, 2020.
- 905 Luo, Y., Pacheco-Labrador, J., Richardson, A. D., Seyednasrollah, B., Perez-Priego, O., Gonzalez-Cascon, R., Martín, M. P.,
906 Moreno, G., Nair, R., Wutzler, T., Bucher, S. F., Carrara, A., Cremonese, E., El-Madany, T. S., Filippa, G., Galvagno, M.,
907 Hammer, T., Ma, X., Martini, D., Zhang, Q., Reichstein, M., Menzel, A., Römermann, C., and Migliavacca, M.: Evergreen
908 broadleaf greenness and its relationship with leaf flushing, aging, and water fluxes, *Agricultural and Forest Meteorology*, 323,
909 109060, <https://doi.org/10.1016/j.agrformet.2022.109060>, 2022.
- 910 Ma, Baldocchi, D. D., Xu, L. K., and Hehn, T.: Inter-annual variability in carbon dioxide exchange of an oak/grass savanna
911 and open grassland in California, *Agricultural and Forest Meteorology*, 147, 157–171,
912 <https://doi.org/10.1016/j.agrformet.2007.07.008>, 2007.
- 913 Ma, S., Baldocchi, D., Wolf, S., and Verfaillie, J.: Slow ecosystem responses conditionally regulate annual carbon balance
914 over 15 years in Californian oak-grass savanna, *Agricultural and Forest Meteorology*, 228–229, 252–264,
915 <https://doi.org/10.1016/j.agrformet.2016.07.016>, 2016a.
- 916 Ma, S., Osuna, J. L., Verfaillie, J., and Baldocchi, D. D.: Photosynthetic responses to temperature across leaf–canopy–
917 ecosystem scales: a 15-year study in a Californian oak-grass savanna, *Photosynth Res*, 132, 277–291,
918 <https://doi.org/10.1007/s11120-017-0388-5>, 2017.
- 919 MacBean, N., Scott, R. L., Biederman, J. A., Peylin, P., Kolb, T., Litvak, M. E., Krishnan, P., Meyers, T. P., Arora, V. K.,
920 Bastrikov, V., Goll, D., Lombardozzi, D. L., Nabel, J. E. M. S., Pongratz, J., Sitch, S., Walker, A. P., Zaehle, S., and Moore,
921 D. J. P.: Dynamic global vegetation models underestimate net CO₂ flux mean and inter-annual variability in dryland
922 ecosystems, *Environ Res Lett*, 16, <https://doi.org/ARTN 094023> 10.1088/1748-9326/ac1a38, 2021.
- 923 Mahecha, Reichstein, M., Lange, H., Carvalhais, N., Bernhofer, C., Grunwald, T., Papale, D., and Seufert, G.: Characterizing
924 ecosystem-atmosphere interactions from short to interannual time scales, *Biogeosciences*, 4, 743–758, <https://doi.org/DOI>
925 10.5194/bg-4-743-2007, 2007.
- 926 Mahecha, M. D., Reichstein, M., Carvalhais, N., Lasslop, G., Lange, H., Seneviratne, S. I., Vargas, R., Ammann, C., Arain,
927 M. A., Cescatti, A., Janssens, I. A., Migliavacca, M., Montagnani, L., and Richardson, A. D.: Global Convergence in the
928 Temperature Sensitivity of Respiration at Ecosystem Level, *Science*, 329, 838–840, <https://doi.org/10.1126/science.1189587>,
929 2010.



- 930 Manzoni, S., Chakrawal, A., Fischer, T., Schimel, J. P., Porporato, A., and Vico, G.: Rainfall intensification increases the
931 contribution of rewetting pulses to soil heterotrophic respiration, *Biogeosciences*, 17, 4007–4023, [https://doi.org/10.5194/bg-](https://doi.org/10.5194/bg-17-4007-2020)
932 17-4007-2020, 2020.
- 933 Martini, D., Pacheco-Labrador, J., Perez-Priego, O., van der Tol, C., El-Madany, T. S., Julitta, T., Rossini, M., Reichstein, M.,
934 Christiansen, R., Rascher, U., Moreno, G., Martin, M. P., Yang, P. Q., Carrara, A., Guan, J. H., Gonzalez-Cascon, R., and
935 Migliavacca, M.: Nitrogen and Phosphorus Effect on Sun-Induced Fluorescence and Gross Primary Productivity in
936 Mediterranean Grassland, *Remote Sens-Basel*, 11, <https://doi.org/ARTN 2562 10.3390/rs11212562>, 2019.
- 937 Mauder, M. and Foken, T.: Documentation and Instruction Manual of the Eddy-Covariance Software Package TK3, 46, 2011.
- 938 Metz, E.-M., Vardag, S. N., Basu, S., Jung, M., Ahrens, B., El-Madany, T., Sitch, S., Arora, V. K., Briggs, P. R., Friedlingstein,
939 P., Goll, D. S., Jain, A. K., Kato, E., Lombardozi, D., Nabel, J. E. M. S., Poulter, B., Séférian, R., Tian, H., Wiltshire, A.,
940 Yuan, W., Yue, X., Zaehle, S., Deutscher, N. M., Griffith, D. W. T., and Butz, A.: Soil respiration–driven CO₂ pulses dominate
941 Australia’s flux variability, *Science*, 379, 1332–1335, <https://doi.org/10.1126/science.add7833>, 2023.
- 942 Migliavacca, Perez-Priego, O., Rossini, M., El-Madany, T. S., Moreno, G., van der Tol, C., Rascher, U., Berninger, A.,
943 Bessenbacher, V., Burkart, A., Carrara, A., Fava, F., Guan, J. H., Hammer, T. W., Henkel, K., Juarez-Alcalde, E., Julitta, T.,
944 Kolle, O., Martin, M. P., Musavi, T., Pacheco-Labrador, J., Perez-Burgueno, A., Wutzler, T., Zaehle, S., and Reichstein, M.:
945 Plant functional traits and canopy structure control the relationship between photosynthetic CO₂ uptake and far-red sun-
946 induced fluorescence in a Mediterranean grassland under different nutrient availability, *New Phytol*, 214, 1078–1091,
947 <https://doi.org/10.1111/nph.14437>, 2017.
- 948 Migliavacca, M., Galvagno, M., Cremonese, E., Rossini, M., Meroni, M., Sonnentag, O., Cogliati, S., Manca, G., Diotri, F.,
949 Busetto, L., Cescatti, A., Colombo, R., Fava, F., Morra Di Cella, U., Pari, E., Siniscalco, C., and Richardson, A. D.: Using
950 digital repeat photography and eddy covariance data to model grassland phenology and photosynthetic CO₂ uptake,
951 *Agricultural and Forest Meteorology*, 151, 1325–1337, <https://doi.org/10.1016/j.agrformet.2011.05.012>, 2011.
- 952 Miller, G. R., Chen, X., Rubin, Y., Ma, S., and Baldocchi, D. D.: Groundwater uptake by woody vegetation in a semiarid oak
953 savanna, *Water Resources Research*, 46, 2009WR008902, <https://doi.org/10.1029/2009WR008902>, 2010.
- 954 Moore, C. E., Beringer, J., Evans, B., Hutley, L. B., and Tapper, N. J.: Tree–grass phenology information improves light use
955 efficiency modelling of gross primary productivity for an Australian tropical savanna, *Biogeosciences*, 14, 111–129,
956 <https://doi.org/10.5194/bg-14-111-2017>, 2017.
- 957 Moreno, G.: Response of understory forage to multiple tree effects in Iberian dehesas, *Agr Ecosyst Environ*, 123, 239–244,
958 <https://doi.org/10.1016/j.agee.2007.04.006>, 2008.
- 959 Morgan, J. A., Parton, W., Derner, J. D., Gilmanov, T. G., and Smith, D. P.: Importance of Early Season Conditions and
960 Grazing on Carbon Dioxide Fluxes in Colorado Shortgrass Steppe, *Rangeland Ecology & Management*, 69, 342–350,
961 <https://doi.org/10.1016/j.rama.2016.05.002>, 2016.
- 962 Morris, K. A., Nair, R. K. F., Moreno, G., Schrumph, M., and Migliavacca, M.: Fate of N additions in a multiple resource-
963 limited Mediterranean oak savanna, *Ecosphere*, 10, <https://doi.org/ARTN e02921 10.1002/ecs2.2921>, 2019.
- 964 Moyano, F. E., Manzoni, S., and Chenu, C.: Responses of soil heterotrophic respiration to moisture availability: An exploration
965 of processes and models, *Soil Biol Biochem*, 59, 72–85, <https://doi.org/10.1016/j.soilbio.2013.01.002>, 2013.



- 966 Nair, R. K. F., Morris, K. A., Hertel, M., Luo, Y. P., Moreno, G., Reichstein, M., Schrumph, M., and Migliavacca, M.: N : P
967 stoichiometry and habitat effects on Mediterranean savanna seasonal root dynamics, *Biogeosciences*, 16, 1883–1901,
968 <https://doi.org/10.5194/bg-16-1883-2019>, 2019.
- 969 Nutini, F., Boschetti, M., Candiani, G., Bocchi, S., and Brivio, P.: Evaporative Fraction as an Indicator of Moisture Condition
970 and Water Stress Status in Semi-Arid Rangeland Ecosystems, *Remote Sensing*, 6, 6300–6323,
971 <https://doi.org/10.3390/rs6076300>, 2014.
- 972 Olschewski, P., Dieng, M. D. B., Moutahir, H., Böker, B., Haas, E., Kunstmann, H., and Laux, P.: Amplified potential for
973 vegetation stress under climate-change-induced intensifying compound extreme events in the Greater Mediterranean Region,
974 *Nat. Hazards Earth Syst. Sci.*, 24, 1099–1134, <https://doi.org/10.5194/nhess-24-1099-2024>, 2024.
- 975 Pacheco-Labrador, J., Perez-Priego, O., El-Madany, T. S., Julitta, T., Rossini, M., Guan, J. H., Moreno, G., Carvalhais, N.,
976 Martin, M. P., Gonzalez-Cascon, R., Kolle, O., Reischstein, M., van der Tol, C., Carrara, A., Martini, D., Hammer, T. W.,
977 Moossen, H., and Migliavacca, M.: Multiple-constraint inversion of SCOPE. Evaluating the potential of GPP and SIF for the
978 retrieval of plant functional traits, *Remote Sens Environ*, 234, <https://doi.org/ARTN 111362 10.1016/j.rse.2019.111362>, 2019.
- 979 Pang, J., Zhao, H., Bansal, R., Bohuon, E., Lambers, H., Ryan, M. H., and Siddique, K. H. M.: Leaf transpiration plays a role
980 in phosphorus acquisition among a large set of chickpea genotypes: Leaf transpiration and P acquisition in chickpea, *Plant
981 Cell Environ*, <https://doi.org/10.1111/pce.13139>, 2018.
- 982 Papale, D., Reichstein, M., Aubinet, M., Canfora, E., Bernhofer, C., Kutsch, W., Longdoz, B., Rambal, S., Valentini, R.,
983 Vesala, T., and Yakir, D.: Towards a standardized processing of Net Ecosystem Exchange measured with eddy covariance
984 technique: algorithms and uncertainty estimation, *Biogeosciences*, 3, 571–583, <https://doi.org/DOI 10.5194/bg-3-571-2006>,
985 2006.
- 986 Pardo, L. H., Fenn, M. E., Goodale, C. L., Geiser, L. H., Driscoll, C. T., Allen, E. B., Baron, J. S., Bobbink, R., Bowman, W.
987 D., Clark, C. M., Emmett, B., Gilliam, F. S., Greaver, T. L., Hall, S. J., Lilleskov, E. A., Liu, L., Lynch, J. A., Nadelhoffer, K.
988 J., Perakis, S. S., Robin-Abbott, M. J., Stoddard, J. L., Weathers, K. C., and Dennis, R. L.: Effects of nitrogen deposition and
989 empirical nitrogen critical loads for ecoregions of the United States, *Ecological Applications*, 21, 3049–3082,
990 <https://doi.org/10.1890/10-2341.1>, 2011.
- 991 Parton, W., Morgan, J., Smith, D., Del Grosso, S., Prihodko, L., Lecain, D., Kelly, R., and Lutz, S.: Impact of precipitation
992 dynamics on net ecosystem productivity, *Global Change Biol*, 18, 915–927, [https://doi.org/10.1111/j.1365-
993 2486.2011.02611.x](https://doi.org/10.1111/j.1365-993), 2012.
- 994 Paulus, S. J., El-Madany, T. S., Orth, R., Hildebrandt, A., Wutzler, T., Carrara, A., Moreno, G., Perez-Priego, O., Kolle, O.,
995 Reichstein, M., and Migliavacca, M.: Resolving seasonal and diel dynamics of non-rainfall water inputs in a Mediterranean
996 ecosystem using lysimeters, *Hydrol Earth Syst Sc*, 26, 6263–6287, <https://doi.org/10.5194/hess-26-6263-2022>, 2022.
- 997 Penuelas, J., Poulter, B., Sardans, J., Ciais, P., van der Velde, M., Bopp, L., Boucher, O., Godderis, Y., Hinsinger, P., Llusia,
998 J., Nardin, E., Vicca, S., Obersteiner, M., and Janssens, I. A.: Human-induced nitrogen-phosphorus imbalances alter natural
999 and managed ecosystems across the globe, *Nat Commun*, 4, <https://doi.org/ARTN 2934 10.1038/ncomms3934>, 2013.
- 1000 Peñuelas, J., Sardans, J., Filella, I., Estiarte, M., Llusà, J., Ogaya, R., Carnicer, J., Bartrons, M., Rivas-Ubach, A., Grau, O.,
1001 Peguero, G., Margalef, O., Pla-Rabés, S., Stefanescu, C., Asensio, D., Preece, C., Liu, L., Verger, A., Rico, L., Barbeta, A.,
1002 Achotegui-Castells, A., Gargallo-Garriga, A., Sperlich, D., Farré-Armengol, G., Fernández-Martínez, M., Liu, D., Zhang, C.,
1003 Urbina, I., Camino, M., Vives, M., Nadal-Sala, D., Sabaté, S., Gracia, C., and Terradas, J.: Assessment of the impacts of
1004 climate change on Mediterranean terrestrial ecosystems based on data from field experiments and long-term monitored field



- 1005 gradients in Catalonia, *Environmental and Experimental Botany*, 152, 49–59,
1006 <https://doi.org/10.1016/j.envexpbot.2017.05.012>, 2018.
- 1007 Perez-Priego, O., Guan, J., Rossini, M., Fava, F., Wutzler, T., Moreno, G., Carvalhais, N., Carrara, A., Kolle, O., Julitta, T.,
1008 Schrupf, M., Reichstein, M., and Migliavacca, M.: Sun-induced chlorophyll fluorescence and photochemical reflectance
1009 index improve remote-sensing gross primary production estimates under varying nutrient availability in a typical
1010 Mediterranean savanna ecosystem, *Biogeosciences*, 12, 6351–6367, <https://doi.org/10.5194/bg-12-6351-2015>, 2015.
- 1011 Petach, A. R., Toomey, M., Aubrecht, D. M., and Richardson, A. D.: Monitoring vegetation phenology using an infrared-
1012 enabled security camera, *Agricultural and Forest Meteorology*, 195–196, 143–151,
1013 <https://doi.org/10.1016/j.agrformet.2014.05.008>, 2014.
- 1014 Piao, S., Wang, X., Wang, K., Li, X., Bastos, A., Canadell, J. G., Ciais, P., Friedlingstein, P., and Sitch, S.: Interannual variation
1015 of terrestrial carbon cycle: Issues and perspectives, *Global Change Biology*, 26, 300–318, <https://doi.org/10.1111/gcb.14884>,
1016 2020.
- 1017 Poulter, B., Frank, D., Ciais, P., Myneni, R. B., Andela, N., Bi, J., Broquet, G., Canadell, J. G., Chevallier, F., Liu, Y. Y.,
1018 Running, S. W., Sitch, S., and van der Werf, G. R.: Contribution of semi-arid ecosystems to interannual variability of the
1019 global carbon cycle, *Nature*, 509, 600–+, <https://doi.org/10.1038/nature13376>, 2014.
- 1020 Reichstein, M., Falge, E., Baldocchi, D., Papale, D., Aubinet, M., Berbigier, P., Bernhofer, C., Buchmann, N., Gilmanov, T.,
1021 Granier, A., Grunwald, T., Havrankova, K., Ilvesniemi, H., Janous, D., Knohl, A., Laurila, T., Lohila, A., Loustau, D.,
1022 Matteucci, G., Meyers, T., Miglietta, F., Ourcival, J. M., Pumpanen, J., Rambal, S., Rotenberg, E., Sanz, M., Tenhunen, J.,
1023 Seufert, G., Vaccari, F., Vesala, T., Yakir, D., and Valentini, R.: On the separation of net ecosystem exchange into assimilation
1024 and ecosystem respiration: review and improved algorithm, *Global Change Biol*, 11, 1424–1439,
1025 <https://doi.org/10.1111/j.1365-2486.2005.001002.x>, 2005.
- 1026 Reichstein, M., Bahn, M., Mahecha, M. D., Kattge, J., and Baldocchi, D. D.: Linking plant and ecosystem functional
1027 biogeography, *P Natl Acad Sci USA*, 111, 13697–13702, <https://doi.org/10.1073/pnas.1216065111>, 2014.
- 1028 Richardson, A. D., Braswell, B. H., Hollinger, D. Y., Jenkins, J. P., and Ollinger, S. V.: Near-surface remote sensing of spatial
1029 and temporal variation in canopy phenology, *Ecological Applications*, 19, 1417–1428, <https://doi.org/10.1890/08-2022.1>,
1030 2009.
- 1031 Richardson, J., Chatterjee, A., and Darrel Jenerette, G.: Optimum temperatures for soil respiration along a semi-arid elevation
1032 gradient in southern California, *Soil Biology and Biochemistry*, 46, 89–95, <https://doi.org/10.1016/j.soilbio.2011.11.008>,
1033 2012.
- 1034 Rolo, V. and Moreno, G.: Interspecific competition induces asymmetrical rooting profile adjustments in shrub-encroached
1035 open oak woodlands, *Trees*, 26, 997–1006, <https://doi.org/10.1007/s00468-012-0677-8>, 2012.
- 1036 Rose, L., Buitenwerf, R., Cramer, M., February, E. C., and Higgins, S. I.: Effects of nutrient supply on carbon and water
1037 economies of C4 grasses, *Functional Plant Biol.*, 45, 935, <https://doi.org/10.1071/FP17359>, 2018.
- 1038 Ruddell, B. L. and Kumar, P.: Ecohydrologic process networks: 1. Identification, *Water Resour Res*, 45, <https://doi.org/Artn>
1039 W03419 10.1029/2008wr007279, 2009.
- 1040 Running, S. W. and Nemani, R. R.: Relating seasonal patterns of the AVHRR vegetation index to simulated photosynthesis
1041 and transpiration of forests in different climates, *Remote Sensing of Environment*, 24, 347–367, <https://doi.org/10.1016/0034->
1042 4257(88)90034-X, 1988.



- 1043 Sardans, J., Rivas-Ubach, A., and Peñuelas, J.: The C:N:P stoichiometry of organisms and ecosystems in a changing world: A
1044 review and perspectives, *Perspectives in Plant Ecology, Evolution and Systematics*, 14, 33–47,
1045 <https://doi.org/10.1016/j.ppees.2011.08.002>, 2012.
- 1046 Sillmann, J., Kharin, V. V., Zhang, X., Zwiers, F. W., and Bronaugh, D.: Climate extremes indices in the CMIP5 multimodel
1047 ensemble: Part 1. Model evaluation in the present climate, *JGR Atmospheres*, 118, 1716–1733,
1048 <https://doi.org/10.1002/jgrd.50203>, 2013.
- 1049 Singh, S. K. and Reddy, V. R.: Combined effects of phosphorus nutrition and elevated carbon dioxide concentration on
1050 chlorophyll fluorescence, photosynthesis, and nutrient efficiency of cotton, *J. Plant Nutr. Soil Sci.*, 177, 892–902,
1051 <https://doi.org/10.1002/jpln.201400117>, 2014.
- 1052 Sippel, S., El-Madany, T. S., Migliavacca, M., Mahecha, M. D., Carrara, A., Flach, M., Kaminski, T., Otto, F. E. L., Thonicke,
1053 K., Vossbeck, M., and Reichstein, M.: Warm Winter, Wet Spring, and an Extreme Response in Ecosystem Functioning on the
1054 Iberian Peninsula, *B Am Meteorol Soc*, 99, S80–S85, <https://doi.org/10.1175/Bams-D-17-0135.1>, 2018.
- 1055 Steiner, B., Scott, R. L., Hu, J., MacBean, N., Richardson, A., and Moore, D. J. P.: Using phenology to unravel differential
1056 soil water use and productivity in a semiarid savanna, *Ecosphere*, 15, e4762, <https://doi.org/10.1002/ecs2.4762>, 2024.
- 1057 Sturtevant, C., Ruddell, B. L., Knox, S. H., Verfaillie, J., Matthes, J. H., Oikawa, P. Y., and Baldocchi, D.: Identifying scale-
1058 emergent, nonlinear, asynchronous processes of wetland methane exchange, *J Geophys Res-Bioge*, 121, 188–204,
1059 <https://doi.org/10.1002/2015jg003054>, 2016.
- 1060 Thieurmél, B.: *suncalc: Compute Sun Position, Sunlight Phases, Moon Position and Lunar Phase*, 2017.
- 1061 Tong, B., Guo, J., Xu, H., Wang, Y., Li, H., Bian, L., Zhang, J., and Zhou, S.: Effects of soil moisture, net radiation, and
1062 atmospheric vapor pressure deficit on surface evaporation fraction at a semi-arid grass site, *Science of The Total Environment*,
1063 849, 157890, <https://doi.org/10.1016/j.scitotenv.2022.157890>, 2022.
- 1064 Tucker, C. J.: Red and photographic infrared linear combinations for monitoring vegetation, *Remote Sensing of Environment*,
1065 8, 127–150, [https://doi.org/10.1016/0034-4257\(79\)90013-0](https://doi.org/10.1016/0034-4257(79)90013-0), 1979.
- 1066 Walther, S., Besnard, S., Nelson, J. A., El-Madany, T. S., Migliavacca, M., Weber, U., Carvalhais, N., Ermida, S. L., Brümmer,
1067 C., Schrader, F., Prokushkin, A. S., Panov, A. V., and Jung, M.: Technical note: A view from space on global flux towers by
1068 MODIS and Landsat: the FluxnetEO data set, *Biogeosciences*, 19, 2805–2840, <https://doi.org/10.5194/bg-19-2805-2022>,
1069 2022.
- 1070 Wang, C. and Tang, Y.: Responses of plant phenology to nitrogen addition: a meta-analysis, *Oikos*, 128, 1243–1253,
1071 <https://doi.org/10.1111/oik.06099>, 2019.
- 1072 Ward, D., Wiegand, K., and Getzin, S.: Walter’s two-layer hypothesis revisited: back to the roots!, *Oecologia*, 172, 617–630,
1073 <https://doi.org/10.1007/s00442-012-2538-y>, 2013.
- 1074 Way, D. A. and Yamori, W.: Thermal acclimation of photosynthesis: on the importance of adjusting our definitions and
1075 accounting for thermal acclimation of respiration, *Photosynth Res*, 119, 89–100, <https://doi.org/10.1007/s11120-013-9873-7>,
1076 2014.
- 1077 Whitecross, M. A., Witkowski, E. T. F., and Archibald, S.: Savanna tree-grass interactions: A phenological investigation of
1078 green-up in relation to water availability over three seasons, *South African Journal of Botany*, 108, 29–40,
1079 <https://doi.org/10.1016/j.sajb.2016.09.003>, 2017.



- 1080 Wingate, L., Ogée, J., Cremonese, E., Filippa, G., Mizunuma, T., Migliavacca, M., Moisy, C., Wilkinson, M., Moureaux, C.,
1081 Wohlfahrt, G., Hammerle, A., Hörtnagl, L., Gimeno, C., Porcar-Castell, A., Galvagno, M., Nakaji, T., Morison, J., Kolle, O.,
1082 Knohl, A., Kutsch, W., Kolari, P., Nikinmaa, E., Ibrom, A., Gielen, B., Eugster, W., Balzarolo, M., Papale, D., Klumpp, K.,
1083 Köstner, B., Grünwald, T., Joffre, R., Ourcival, J.-M., Hellstrom, M., Lindroth, A., George, C., Longdoz, B., Genty, B., Levula,
1084 J., Heinesch, B., Sprintsin, M., Yakir, D., Manise, T., Guyon, D., Ahrends, H., Plaza-Aguilar, A., Guan, J. H., and Grace, J.:
1085 Interpreting canopy development and physiology using a European phenology camera network at flux sites, *Biogeosciences*,
1086 12, 5995–6015, <https://doi.org/10.5194/bg-12-5995-2015>, 2015.
- 1087 Wood, J. D., Griffis, T. J., and Baker, J. M.: Detecting drift bias and exposure errors in solar and photosynthetically active
1088 radiation data, *Agricultural and Forest Meteorology*, 206, 33–44, <https://doi.org/10.1016/j.agrformet.2015.02.015>, 2015.
- 1089 Wutzler, T., Lucas-Moffat, A., Migliavacca, M., Knauer, J., Sickel, K., Sigut, L., Menzer, O., and Reichstein, M.: Basic and
1090 extensible post-processing of eddy covariance flux data with REddyProc, *Biogeosciences*, 15, 5015–5030,
1091 <https://doi.org/10.5194/bg-15-5015-2018>, 2018.
- 1092 Xu, L. and Baldocchi, D. D.: Seasonal trends in photosynthetic parameters and stomatal conductance of blue oak (*Quercus*
1093 *douglasii*) under prolonged summer drought and high temperature, *Tree Physiology*, 23, 865–877,
1094 <https://doi.org/10.1093/treephys/23.13.865>, 2003.
- 1095 Yamori, W., Hikosaka, K., and Way, D. A.: Temperature response of photosynthesis in C3, C4, and CAM plants: temperature
1096 acclimation and temperature adaptation, *Photosynth Res*, 119, 101–117, <https://doi.org/10.1007/s11120-013-9874-6>, 2014.
- 1097 Yan, D., Scott, R. L., Moore, D. J. P., Biederman, J. A., and Smith, W. K.: Understanding the relationship between vegetation
1098 greenness and productivity across dryland ecosystems through the integration of PhenoCam, satellite, and eddy covariance
1099 data, *Remote Sensing of Environment*, 223, 50–62, <https://doi.org/10.1016/j.rse.2018.12.029>, 2019.
- 1100 Yiou, P., Sornette, D., and Ghil, M.: Data-adaptive wavelets and multi-scale singular-spectrum analysis, *Physica D*, 142, 254–
1101 290, [https://doi.org/Doi.10.1016/S0167-2789\(00\)00045-2](https://doi.org/Doi.10.1016/S0167-2789(00)00045-2), 2000.
- 1102 Zhang, L., Wylie, B. K., Ji, L., Gilmanov, T. G., and Tieszen, L. L.: Climate-Driven Interannual Variability in Net Ecosystem
1103 Exchange in the Northern Great Plains Grasslands, *Rangeland Ecology & Management*, 63, 40–50, <https://doi.org/10.2111/08-1104>, 2010.
- 1105 Zhang, Y., Xiao, X., Guanter, L., Zhou, S., Ciais, P., Joiner, J., Sitch, S., Wu, X., Nabel, J., Dong, J., Kato, E., Jain, A. K.,
1106 Wiltshire, A., and Stocker, B. D.: Precipitation and carbon-water coupling jointly control the interannual variability of global
1107 land gross primary production, *Sci Rep*, 6, 39748, <https://doi.org/10.1038/srep39748>, 2016.